JAAS

Journal of Analytical Atomic Spectrometry

Accepted Manuscript

This article can be cited before page numbers have been issued, to do this please use: M. A. Reis, *J. Anal. At. Spectrom.*, 2025, DOI: 10.1039/D4JA00463A.

View Article Online
DOI: 10.1039/D4JA00463A

Multilayer targets PIXE spectra simulation (X,X) secondary fluorescence corrections algorithm

M. A. Reis[a,b*]

a. C^{2}TN, Dept. Eng. e Ciências Nucleares, Instituto Superior Técnico, Univ.de Lisboa, CTN, EN10, km139.7, 2695-066 Bobadela LRS, Portugal

b. Ad Fisicateca, R. Pedro Vaz Henriques, 7, 2560-256 Torres Vedras, Portugal

Contents

Keywords:
Secondary fluorescence, Simulation, PIXE, Equivalent thickness

Abstract

Simulation of particle induced X-ray emission (PIXE) spectra is not a recent subject. Still, when samples are not homogeneous problems emerge even in the most simple case of layered samples. If it is necessary to consider the presence of the same chemical element in more than one physically distinct layer the number of available simulation codes is very small. In addition, although X-ray emission spectra from PIXE experiments are much less prone to significant secondary fluorescence issues than their X-ray Fluorescence Spectrometry (XRF) counterpart, cases emerge where secondary fluorescence calculations are necessary to assure good PIXE spectra simulations, even if corrections are small. The case of secondary fluorescence induced by primary X-rays in thick homogeneous samples was solved long ago by various authors. In the case of non-homogenous targets, the problem becomes much more complex and, although also addressed long ago, a general solution is not possible to find in standard access literature for the PIXE technique case. In the present work we revise a secondary fluorescence correction method presented in 1996 to handle homogeneous targets and extend it to be applicable to multilayered targets. Its implementation in the DT2 code allows to simulate PIXE spectra taking into account these type of matrix effects correction in complex multilayer targets. Fluorescence between different physical layers, the possibility of the presence of one chemical element in more than one layers, and the potential "*illusional*" presence of a chemical element in a given layer due to the secondary fluorescence effects, when its real concentration in that layer is null, are dealt with. This is the first of what aims to be a series of three papers. In this part I work, the model is presented for the case of secondary X-rays induced by primary X-rays produced by particle collisions. Applications and potentially demanding experimental conditions will be dealt with in part II, and the case of secondary X-rays induced by non-radiative transitions primary radiation of fast electrons will be addressed in part III.

*Corresponding author. Tel.: +351 219946107; Email address: mareis@ctn.tecnico.ulisboa.pt

View Article Online
DOI: 10.1039/D4JA00463A

1 Introduction

Quantitative work on particle induced X-ray emission (PIXE)[?] can be made in a very simple approximation if the targets are thin enough so that the ion beam particles impacting in the target do not loose any significant amount of energy while crossing it and the sample elements characteristic X-rays are well separated in the spectra. In this case, if standard samples have been previously analysed in the same conditions, integrating the characteristic X-ray peaks, or even just using its height, will provide quantitative data without any need for much complex processing[?].

Still, in many cases the situation is not so simple. If the target is not thin enough, the target X-ray yield must be determined by integration of the yield function along the ion beam particles path in the target, and it can even happen that enhancement of X-ray emission relative to the yield expected from particle induced ionizations takes place. In *"standard"* cases, as mentioned by Folkmann in 1974[?], it is important to consider the fluorescence processes that result from the absortion of primary X-rays (the X-rays induced directly by particle colisions), in particular those cases that result from the absorption of the primary characteristic X-rays in the sample material. This absoprtion is named self-absorption, and the fluorescence procresses are usually refered to as secondary fluorescence, and are probably the most important phenomena leading to this enhancement.

Being quite significant when studying some types (eg: metal alloys) of thick targets (targets that are thick enough to completely stop the incident ion beam), the X-ray yield enhancement effect due to secondary fluorescence was addressed long ago by several authors and solved for the case of homogeneous thick samples. In the case of PIXE work, Reuter et al. in 1975[?], Ahlberg in 1977[?] and Richter and Wätjen in 1981[?] presented analytical solutions to the problem, Van Oystaeyen and Demortier in 1983[?] developed a Monte Carlo method, Campbell et al. in 1989[?] calculated the need for terciary corrections and Ryan et al., in the beginning of the 1990s[? ?], implemented in GeoPIXE calculation processes to deal with thin layers and inclusions in complex geological samples.

The secondary fluorescence effect in PIXE is similar to what is observed in X-ray Fluorescence Spectrometry (XRF), and therefore some of these methods resemble and reflect the 1960s work of Shiraiwa and Fujino[?], even though the primary yield determination in the case of PIXE cannot be handle simply as an exponential term and must be found by numerical calculation, which complicates all further calculations.

In the beginning of the 1990s decade the issue was revisited by my self while developing the first version of the DATTPIXE package[?]. After a first approach based on the work of Ahlberg[?], a variant was developed taking the model of Richter and Wätjen[?] as a working base to define a function of depth term for the secondary fluorescence correction, which can be added to the primary X-ray yield prior to integration along the particles penetration path. This model then named "penetration function model", as presented in 1996[?], was applicable for thick and half-thick targets and was implemented as such in the DATTPIXE package 1996 version[?].

As mentioned above, PIXE samples are considered thin if it is possible to assume that the energy loss of incoming particles after crossing the target is negligible. In practice, in many cases, this energy loss is not negligible and the samples must be considered either half-thick, if the beam particles emerge from the target, or thick if they are completely stopped inside it.

If the samples are not homogeneous in depth the simplest case that can be considered is that of layered targets. These being targets that can be modeled as a set of physically distinct layers, each of them being a thin or half-thick target that is crossed by the particles of the beam, which may in the end be stopped in a thick substrate on top of which the layers are successsively present. In this case, a situation more complex is faced both for yield calculation and even more for cases where the secondary fluorescence effect must be accounted for.

In the case of XRF, the handling of secondary fluorescence effects in layered targets has been described in detail by De Boer[?]. In this case, since the primary and secondary excitation processes are identical, major correction terms may be expected in several cases since the ionization cross-section of the radiation inducing secondary fluorescence is higher than the corresponding ionization cross-section of the ionization X-ray beam.

This is not the case in PIXE, since the particle collisions ionization cross-sections of matrix atoms are, in most (if not all) of the cases, higher or even much higher than the ionization cross-sections of matrix atoms by the primary X-rays produced after the particle collisions.

In many cases, in PIXE experiments, secondary fluorescence enhancement effects in layered targets can, therefore, be negleted since it is reasonably possible to assume that any possiblle correction is very small. Nevertheless, since the PIXE technique is becoming more and more used to study layered targets, frequently using a Total-IBA[?] approach, complex problems start to emerge and secondary fluorescence calculations in layered targets can no longer be disregarded, even if just to assure that they are small.

Although, also for PIXE, the problem of secondary fluorescence effects in non-homogeneous samples has been addressed since the beginning of the 1990s[? ?], still, a systematic and detailed description of the general PIXE case of layered targets, similar to De Boer's work for XRF, could not be found in standard accessible literature, even though it is mentioned in Ryan et al. 1990s papers as "*in preparation*".

Besides this difficulty in finding calculation details on the 1990s work in the subject, the present paper focus on PIXE spectra simulation, while previous work has so far focused on calculating changes that must be taken into account to fit spectra details. In fact, although the two goals share a significant fraction of problems, not all of them are exactly the same and the best solutions for one and other issues are also not fully coincident.

In this work, we revisit the secondary fluorescence correction *penetration function model* published in 1996[?] for homogeneous thick and half-thick targets and extend it to include layered targets.

No limitation is set on the presence of elements in layers, meaning that elements may be repeated in different physical layers and/or generate secondary X-ray due to primary radiation originated in layers where they are not physically present, in which cases the "*illusion*" of an element being present where the primary radiation is originated may emerge.

Finally, to assure that details on changes in relative intensities of various transitions to the same sub-shell are properly dealt with, calculations and integration over the multilayers structure are carried out for each transition individually.

Taking into account the complexity of the problem, in this work the presentation is limited to the description of the model in the case where secondary X-rays are induced by primary characteristic X-rays, and to its implementation in the DT2 package[? ? ? ?]. In related works, to be published in a near future (parts II and III), applications and the problem of secondary X-rays induced by electrons provenent from the non-radiative transitions following the initial collision of beam particles, will be addressed.

2 PIXE target X-ray yield

2.1 Thin targets

When considering thin targets under particles irradiation, the number of X-rays, N_{j,Z_i}, detected from rearrangement transitions j (K_α , L_α , ...) of element Z_i can be written as:

$$N_{j,Z_i} = \frac{\Omega}{4\pi}\, \varepsilon_{\det,j}\, T_{sis,j}\, N_p\, C_{pp}(E_p)\, b_{cs}\, \mathscr{Y}^{tot}_{j,Z_i} \tag{1}$$

being

$$\mathscr{Y}^{tot}_{j,Z_i}(E_p) = \frac{\mathscr{C}_{part}}{M_{at,Z_i}}\, \sigma^X_{j,Z_i}(E_p)\, \frac{\xi}{cos(\psi_{inc})}\, f_{Z_i} \tag{2}$$

where

$$\mathscr{C}_{part} = \frac{N_{Av}\cdot(barn/cm^2)}{\text{particle charge in } \mu C\cdot(g/\mu g)} \quad \text{, being for protons} \quad \mathscr{C}_{part} = 3.75872462\times10^6$$

$\frac{\Omega}{4\pi}$ is the detector solid angle fraction, $\varepsilon_{\det,j}$ and $T_{sis,j}$ are the energy dependent detector efficiency and the transmission coefficient of the absorbers placed between the sample and the detector, respectively, for the X-rays emitted by transitions j of element Z_i. N_p is the number of particles used in the irradiation, C_{pp} is the charge per particle in μC, b_{cs} is the particles beam cross-section and ψ_{inc} is the incidence angle defined between the beam direction and the normal to the target surface.

$\mathscr{Y}^{tot}_{j,Z_i}(E_p)$ is the target total X-ray yield, for transition j of element Z_i, per μC for a target irradiated by E_p energy particles, which includes the mass fraction of element Z_i in the target, f_{Z_i}. Finaly, N_{Av} is the Avogadro's number, M_{at,Z_i} the molar mass of element Z_i, $\sigma^X_{j,Z_i}(E_p)$ the X-ray production cross-section in barn for particles of energy E_p and ξ is the sample areal mass in $\mu g/cm^2$, frequently refered as thickness even though it does not have dimensions of a distance. The value of $\mathscr{C}_{part}$ has been calculated from the revised SI standard based on the 2017 CODATA revision[?].

It is important to emphasize here that the mass fraction, f_{Z_i}, of element Z_i is not included in ξ, but kept separate in purpose both for the possibility of being assumed as an unknown in analytical processes, as well as a parameter for system calibration operations.

2.2 The equivalent thickness concept

When dealing with thick or half-thick targets, the calculation of the total X-ray target yield is not so straight forward. In these cases, as the ion beam particles penetrate the target, they loose energy, which changes their X-ray production cross-section, $\sigma^X_{j,Z_i}(E_p)$, since E_p is reduced, and the induced X-rays are absorbed before exiting the sample. The target total X-ray yield for any transition j originating from any element Z_i must now be determined by integrating the differential effective yield density. Still, introducing the concept of *equivalent thickness*[?], $\xi_{eq,j,Z_i}(E_p)$,

$$\xi_{eq,j,Z_i}(E_p) = \int_{E_p}^{E_{out}} \frac{\sigma^X_{j,Z_i}(E)}{\sigma^X_{j,Z_i}(E_p)}\, \frac{T_{j,Z_i}(x(E))}{S(x)}\, dE = \int_0^{x(E_{out})} \frac{\sigma^X_{j,Z_i}(E(x))}{\sigma^X_{j,Z_i}(E_p)}\, T_{j,Z_i}(x)\, dx \tag{3}$$

eq(**??**) still allows to calculate the target total X-ray yield, $\mathscr{Y}^{tot}_{j,Z_i}(E_p)$, for thick and half-thick targets as:

$$\mathscr{Y}^{tot}_{j,Z_i}(E_p) = \frac{\mathscr{C}_{part}}{M_{at,Z_i}}\, \sigma^X_{j,Z_i}(E_p)\, \xi_{eq,j,Z_i}(E_p) \tag{4}$$

In eq(**??**) $x(E)$ is the *penetration depth variable* defined as the distance of a given point along the particles penetration path and the sample surface, measured along the ion beam path.

$T_{j,Z_i}(x(E)) \equiv T_{j,Z_i}(x)$ is the absorption of X-rays j of element Z_i while travelling from penetration depth $x \equiv x(E)$ to the surface of the sample, and $S(x(E)) = \frac{dE_p}{dx}$ is the ion beam particles energy loss derivative.

Normalizing to the incident energy X-ray production cross-section allows to formally write the total thick target yield in the same way as for thin targets by replacing the target thickness by the equivalent thickness. The main difference being that, while the thin target surface area is independent of the X-ray being measured, the equivalent thickness is different for every different X-ray.

View Article Online
DOI: 10.1039/D4JA00463A

2.3 Non-homogeneous targets

The use of the *equivalent thickness* concept allows to extend the expression of the target total X-ray yield, even for the general multilayer case. Still, it is important to realize that now the elements mass fraction in each layer must be also included in the definition because it changes from layer to layer.

Making T^n_{j,Z_i} the transmission of element Z_i j transition X-rays from layer n to the surface the result is:

$$\mathscr{Y}^{tot,ml}_{j,Z_i}(E_p) = \frac{\mathscr{C}_{part}}{M_{at,Z_i}}\ \sigma^X_{j,Z_i}(E_p)\,\xi^{ml}_{eq,j,Z_i}(E_p) \tag{5}$$

$$\xi^{ml}_{eq,j,Z_i}(E_p) = \sum_{m=1}^{All\ layers}\left(\prod_{n=1}^{m-1} T^n_{j,Z_i}\right)\frac{\sigma^X_{j,Z_i}\left(E^m_p\right)}{\sigma^X_{j,Z_i}(E_p)}\, f_{Z_i,m}\int_{x_0^m}^{x^m_{(E_{out})}}\frac{\sigma^X_{j,Z_i}(E(x))}{\sigma^X_{j,Z_i}\left(E^m_p\right)}\ T_{j,Z_i}(x)\ dx \tag{6}$$

Last but not necessarily least, even if the sample is not laterally homogeneous and/or if the detector size or detector sample distance leads to transmission terms or layer structure description that depends on an y,z positioning of the beam on the sample, the concept although becomming a bit abstract, can still be used to establish the following general expression for PIXE target yield of general targets irradiated by particles of E_p energy, if a set of homogeneous (y_a,z_b) regions can be established to describe the sample:

$$N_{j,Z_i}(E_p) = \sum_{(y_a,z_b)=1}^{All\ (y_a,z_b)\ pairs}\frac{\Omega^{(y_a,z_b)}}{4\pi}\ \varepsilon^{(y_a,z_b)}_{\det,j}\ T^{(y_a,z_b)}_{sis,j}\ N_p^{(y_a,z_b)}\ C_{pp}(E_p)\,b_{cs}\ \mathscr{Y}^{ml,(y_a,z_b)}_{j,Z_i} \tag{7}$$

being

$$\mathscr{Y}^{ml,(y_a,z_b)}_{j,Z_i}(E_p) = \frac{\mathscr{C}_{part}}{M_{at,Z_i}}\ \sigma^X_{j,Z_i}(E_p)\,\xi^{ml,(y_a,z_b)}_{eq,j,Z_i}(E_p) \tag{8}$$

and

$$\xi^{ml,(y_a,z_b)}_{eq,j,Z_i}(E_p) = \sum_{m_{(y_a,z_b)}=1}^{All\ layers}\left(\prod_{n_{(y_a,z_b)}=1}^{m_{(y_a,z_b)}-1} T^{n_{(y_a,z_b)}}_{j,Z_i}\right)\frac{\sigma^X_{j,Z_i}\left(E_p^{m_{(y_a,z_b)}}\right)}{\sigma^X_{j,Z_i}(E_p)}\, f^{m_{(y_a,z_b)}}_{Z_i}\,.$$

$$\cdot\int_{x_0^{m_{(y_a,z_b)}}}^{x^{m_{(y_a,z_b)}}_{(E_{out})}}\frac{\sigma^X_{j,Z_i}(E(x))}{\sigma^X_{j,Z_i}\left(E_p^{m_{(y_a,z_b)}}\right)}\ T^{m_{(y_a,z_b)}}_{j,Z_i}(x)\ dx \tag{9}$$

3 Secondary fluorescence penetration function model

3.1 Primary point emission and cylindrical symmetry

Consider fig.**??** representing an homogenous target. As the ion beam particles penetrate the target, at any given penetration depth x_1, X-rays are induced and emitted in all directions. A fraction of these, say B^{prim}_β, follows in the direction of the detector, while others, say A_α, are emitted in another direction and may be absorbed in the target material, say in volume dV at a distance r from the x_1 position, and also induce the emission of B_β X-rays, which may well be emitted in the direction of the detector and contribute, with say B^{sec}_β X-rays to the B_β peak in the measured spectrum. In this case, the A_α and B_β X-rays produced at x_1 position are named *primary X-rays*. The B_β X-rays produced in volume dV at position $\vec{x_1}+\vec{r}$, are named *secondary fluorescence X-rays*, and some of these may add to the primary B_β X-rays reaching the X-ray detector, enhancing the target total X-ray yield for B_β X-rays.

Fig.**??**(a), represents the ion beam incident in a direction that may be not contained in the detection plane defined by the normal to the sample surface (shown in yelow in both fig.**??**(a) and (b)) and the line connecting point x_1 and the detector. Assuming that any relevant distance r is small relative to the distance between x_1 and the detector, so that ψ_{det} can be assumed as constant and independent of r, the circular symmetry around the sample normal can be assumed for all the detection processes, even if the irradiation beam is not in the detection plane. This is so because the point x_1 is the single common point to both irradiation and detection processes. Furthermore, if the target can be considered lateral homogeneous (meaning that layers are infinite and homogeneous in the planes parallel to the sample surface), all points x_n (along the beam path) outside of the detection plane may be assumed, for all calculation purposes, as equivalente to its projection (x'_n) on the sample normal.

In the case of complex wide angle detector geometries the whole approach still applies, although numerical integration over the various ψ_{det} values will now be required.

The need for numerical integration in these cases, is not a restriction of the secondary fluorescence correction process, but is also required to properly determine matrix corrections processes affecting the primary X-ray yield, as mentioned in the previous section.

3.2 Secondary X-ray fluorescence cross-section

In order to determine the total amount of secondary B^{sec}_β X-rays, it is necessary to start by writing the differential density function, $dX_{B_\beta A\alpha}(x_1)$, describing the conversion of X-rays A_α produced at a penetration depth x_1 in secondary X-rays B_β (the "sec"

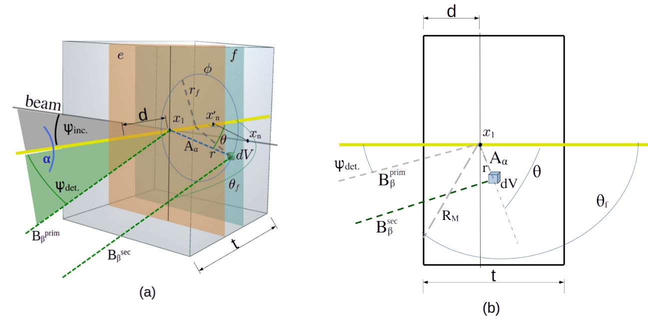

Figure 1 Primary X-rays A_α produced at a penetration depth x_1 lead to the emission of secondary X-rays B_β in volume dV that add to primary B_β X-rays, enhancing their target yield. The X-ray emission process is assumed to have cylindrical symmetry and therefore be possible to describe using a simple 2D image (right). This is so, even if the ion beam direction is outside the detection plane defined by the sample normal (in yelow in the images) and the direction defined by x_1 and the detector. Angle α between the incidence plane defined by the beam and the sample normal (left image) and the detection plane can take any value (check main text for details). Still, for the calculations presented to be valid, it must be possible to assume the samples as infinite and homogeneous in the plane perpendicular to the sample normal (eg: planes e and f in the left image).

uperscript will be omitted for simplicity of writing) that reach the target surface after being induced in the volume element dV. The following expression may be used as starting point:

$$dX_{B_\beta}(A_\alpha;x_1) = \mathscr{P}^X_{A\alpha}(E(x_1))\ T_{B_\beta}(x_1,r,\theta)\ \mathscr{R}^\eta_{B_\beta}(A_\alpha)\ \mathscr{Q}_{A\alpha}(x_1,r)\ dV \tag{10}$$

where:

- $\mathscr{P}^X_{A\alpha}(E(x_1)) = \sigma^X_{A\alpha,Z_i}(E(x_1))\,f_A$ is the primary A_α X-rays production density function at penetration depth x_1;
- $T_{B_\beta}(x_1,r,\theta)$ is the transmission factor of B_β X-rays from the volume dV up to the target surface, calculated for the detectors direction.
- $\mathscr{R}^\eta_{B_\beta}(A_\alpha)$ is the conversion probability that A_α X-rays absorbed in element B in sub-shell η are converted in B_β secondary X-rays;

  and
- $\mathscr{Q}_{A\alpha}(x_1,r)$ is the cross-section for A_α X-ray to be absorbed at a distance r away from the emission point x_1.

The primary X-ray production term corresponds to the differential terms in the expressions presented in the previous sections, which was also partially addressed in the previous subsection.

It remains therefore to discuss the other terms, which product may be refered to as the secondary fluorescence cross-section for the conversion of A_α primary X-rays in B_β secondary X-rays.

Still, before any other discussion it is necessary to deal with is the lack of an explicit term on element B mass fraction, f_B, in eq(**??**), which is needed to be possible to add to eq(**??**), the term resulting from this exercise, to obtain a proper expression for an equivalent thickness secondary fluorescence correction, since $\xi_{eq,j,Z_i}(E_p)$ has no mass term.

3.2.1 $\mathscr{R}^\eta_{\rho B_\beta}(A_\alpha)$ and $\mu^\eta_{\rho B_\beta}(A_\alpha)$ specific conversion probability

Obtaining this explicit mass term can be made by factoring out the $\mathscr{R}^\eta_{B_\beta}(A_\alpha)$ conversion probability component. Only the cases where the absorbing and emitting shell of B are the same will be considered, because the number of secondary B_β X-rays emitted from transitions to a shell different from the shell absorbing the primary A_α X-rays is, in most cases, not relevant when compared to the primary B_β X-rays produced in that shell. The cases where this is not valid are just the situations where the ion beam particles either do not reach the fluorescence layer containing the emitter of the B_β X-rays, or reach it having already lost most of its energy, while the B_β X-rays can still significantly emerge from the sample towards the detector. A condition which is probably extremely rare in practice.

This being set, the factoring out of the $\mathscr{R}^\eta_{B_\beta}(A_\alpha)$ term in the simplest case, an absorbing K-shell, can be obtained based in the following result:

$$\mathscr{R}^K_{B_\beta}(A_\alpha) = \lim_{\triangle r\to 0}\frac{\left(1-e^{-\sigma^{photo}_B(A_\alpha)f_{B_\beta}\triangle r}\right)}{\left(1-e^{-\mu_{A\alpha}\triangle r}\right)}\ \omega_{K,B}\ k_{\beta,B} \Rightarrow \mathscr{R}^K_{B_\beta}(A_\alpha) = \frac{\sigma^{photo}_{K,B}(A_\alpha)\ \omega_{K,B}\ k_{\beta,B}}{\mu_{A_\alpha}}\ f_B \tag{11}$$

where $\sigma^{photo}_{K,B}(A_\alpha)$ is the K-shell photoelectric ionization cross-section of B for A_α X-rays, $\omega_{K,B}$ is the K-shell fluorescence coefficient of B and $k_{\beta,B}$ is the branch ratio of transition β out of all radiative transitions to the K-shell of the B element.

View Article Online
DOI: 10.1039/D4JA00463A

The mass fraction term, f_B, can now be factored out in order to establish a specific probability, $\mu^K_{\rho B_\beta}(A_\alpha)$, independent of both the mass fraction and the mass absorption coefficient of the A_α X-rays, namely:

$$\mu^K_{\rho B_\beta}(A_\alpha) = \mu_{A_\alpha}\frac{\mathscr{R}^K_{B_\beta}(A_\alpha)}{f_{B_\beta}} = \sigma^{photo}_{K,B}(A_\alpha)\ \omega_{K,B}\ k_{\beta,B} \Rightarrow \mathscr{R}^\eta_{B_\beta}(A_\alpha) = \frac{\mu^\eta_{\rho B_\beta}(A_\alpha)}{\mu_{A_\alpha}}\ f_{B_\beta} \quad (12)$$

Eq(**??**) can now be written having f_{B_β} factored out, namely as:

$$dX_{B_\beta}(A_\alpha;x_1) = \mathscr{P}^X_{A\alpha}(E(x_1))\ f_{B_\beta}\ T_{B_\beta}(x_1,r,\theta)\ \frac{\mu^\eta_{\rho B_\beta}(A_\alpha)}{\mu_{A_\alpha}}\ \mathscr{Q}_{A_\alpha}(x_1,r)\ dV \quad (13)$$

In the case of L and M sub-shells the situation is a bit more complex, nevertheless, the same reasoning as used for the K-shell applies since changes are only present in the photoelectric cross-section term. The generalization of eq(**??**), defining $\mu^\eta_{\rho B_\beta}(A_\alpha)$, can therefore be made.

K, L and M sub-shells photoelectric ionization cross section are normally approximated[? ?] based on the total absorption cross section of the X-ray energy, $\sigma_{T,B}(A_\alpha) \equiv \mu_{A_\alpha}$, and the jump ratios, S_η, for the sub-shell. Taking E_i to be the X-ray or the sub-shell ionization energy, as applicable, the following results apply to the K, L and M sub-shells fluorescence (omitting the A_α term for simplicity):

$$\text{if } E_K < E_{A_\alpha}\quad \sigma^{photo}_K = \frac{S_K-1}{S_K}\ \sigma_{T,B} \quad ; \quad \mu^K_{\rho B_\beta} = \sigma^{photo}_{K,B}\ \omega_{K,B}\ k_{\beta,B} \quad (14)$$

if $E_{L1} < E_{A_\alpha} < E_K$

$$\sigma^{photo}_{L3,B} = \frac{S_{L3}-1}{S_{L3}S_{L2}S_{L1}}\sigma_{T,B}\ ;\ \sigma^{photo}_{L2,B} = \frac{S_{L2}-1}{S_{L2}S_{L1}}\sigma_{T,B}\ ;\ \sigma^{photo}_{L1,B} = \frac{S_{L1}-1}{S_{L1}}\sigma_{T,B} \quad (15)$$

$$\mu^{L3}_{\rho B_\beta} = \left[(f_{L12}f_{L23}+f_{L13})\sigma^{photo}_{L1,B} + f_{L23}\sigma^{photo}_{L2,B} + \sigma^{photo}_{L3,B}\right]\ \omega_{L3,B}\ k_{\beta,B} \quad (16)$$

$$\mu^{L2}_{\rho B_\beta} = \left(f_{L12}\sigma^{photo}_{L1,B} + \sigma^{photo}_{L2,B}\right)\ \omega_{L2,B}\ k_{\beta,B}\ ;\ \mu^{L1}_{\rho B_\beta} = \sigma^{photo}_{L1,B}\ \omega_{L1,B}\ k_{\beta,B} \quad (17)$$

if $E_{L2} < E_{A_\alpha} < E_{L1}$

$$\sigma^{photo}_{L3,B} = \frac{S_{L3}-1}{S_{L3}S_{L2}}\ \sigma_{T,B}\ ;\ \sigma^{photo}_{L2,B} = \frac{S_{L2}-1}{S_{L2}}\ \sigma_{T,B} \quad (18)$$

$$\mu^{L3}_{\rho B_\beta} = \left(f_{L23}\sigma^{photo}_{L2,B} + \sigma^{photo}_{L3,B}\right)\ \omega_{L3,B}\ k_{\beta,B}\ ;\ \mu^{L2}_{\rho B_\beta} = \sigma^{photo}_{L2,B}\ \omega_{L2,B}\ k_{\beta,B} \quad (19)$$

if $E_{L3} < E_{A_\alpha} < E_{L2}$

$$\sigma^{photo}_{L3,B} = \frac{S_{L3}-1}{S_{L3}}\ \sigma_{T,B}\quad ;\quad \mu^{L3}_{\rho B_\beta} = \sigma^{photo}_{L3,B}\ \omega_{L3,B}\ k_{\beta,B} \quad (20)$$

if $E_{M1} < E_{A_\alpha} < E_{L3}$

$$\sigma^{photo}_{Mj,B} = \frac{S_{Mj}-1}{\Pi^j_{i=1}(S_{Mi})}\sigma_{T,B}\ \text{ for } j\in[2,5]\ ;\ \sigma^{photo}_{M1,B} = \frac{S_{M1}-1}{(S_{M1})}\sigma_{T,B} \quad (21)$$

$$\begin{aligned}\mu^{M5}_{\rho B_\beta} = \Big[&(f_{M13}f_{M34}f_{M45}+f_{M13}f_{M35}+f_{M14}f_{M45}+f_{M15})\sigma^{photo}_{M1,B} + \\ &+(f_{M12}f_{M23}f_{M34}f_{M45}+f_{M12}f_{M23}f_{M35}+f_{M12}f_{M24}f_{M45})\sigma^{photo}_{M1,B} + \\ &+(f_{M23}f_{M34}f_{M45}+f_{M23}f_{M35}+f_{M24}f_{M45}+f_{M25})\sigma^{photo}_{M2,B} + \\ &+(f_{M34}f_{M45}+f_{M35})\sigma^{photo}_{M3,B} + f_{M45}\ \sigma^{photo}_{M4,B} + \sigma^{photo}_{M5,B}\Big]\omega_{M5,B}\ k_{\beta,B}\end{aligned} \quad (22)$$

$$\begin{aligned}\mu^{M4}_{\rho B_\beta} = \Big[&(f_{M12}f_{M23}f_{M34}+f_{M12}f_{M24}+f_{M13}f_{M34}+f_{M14})\sigma^{photo}_{M1,B} + \\ &+(f_{M23}f_{M34}+f_{M24})\sigma^{photo}_{M2,B} + f_{M34}\ \sigma^{photo}_{M3,B} + \sigma^{photo}_{M4,B}\Big]\omega_{M4,B}\ k_{\beta,B}\end{aligned} \quad (23)$$

$$\mu^{M3}_{\rho B_\beta} = \left[(f_{M12}f_{M23}+f_{M13})\sigma^{photo}_{M1,B} + f_{M23}\ \sigma^{photo}_{M2,B} + \sigma^{photo}_{M3,B}\right]\omega_{M3,B}\ k_{\beta,B} \quad (24)$$

$$\mu^{M2}_{\rho B_\beta} = \left(f_{M12}\sigma^{photo}_{M1,B} + \sigma^{photo}_{M2,B}\right)\omega_{M2,B}\ k_{\beta,B}\quad ;\quad \mu^{M1}_{\rho B_\beta} = \sigma^{photo}_{M1,B}\ \omega_{M1,B}\ k_{\beta,B} \quad (25)$$

if $E_{M2} < E_{A_\alpha} < E_{M1}$

$$\sigma^{photo}_{Mj,B} = \frac{S_{Mj}-1}{\Pi^j_{i=1}(S_{Mi})}\sigma_{T,B}\ \text{ for } j\in[3,5]\ ;\ \sigma^{photo}_{M2,B} = \frac{S_{M2}-1}{(S_{M2})}\sigma_{T,B} \quad (26)$$

$$\begin{aligned}\mu^{M5}_{\rho B_\beta} = \Big[&(f_{M23}f_{M34}f_{M45}+f_{M23}f_{M35}+f_{M24}f_{M45}+f_{M25})\sigma^{photo}_{M2,B} + \\ &+(f_{M34}f_{M45}+f_{M35})\sigma^{photo}_{M3,B} + f_{M45}\ \sigma^{photo}_{M4,B} + \sigma^{photo}_{M5,B}\Big]\omega_{M5,B}\ k_{\beta,B}\end{aligned} \quad (27)$$

$$\mu^{M4}_{\rho B_\beta} = \left[(f_{M23}f_{M34}+f_{M24})\sigma^{photo}_{M2,B} + f_{M34}\ \sigma^{photo}_{M3,B} + \sigma^{photo}_{M4,B}\right]\omega_{M4,B}\ k_{\beta,B} \quad (28)$$

$$\mu^{M3}_{\rho B_\beta} = \left[f_{M23}\ \sigma^{photo}_{M2,B} + \sigma^{photo}_{M3,B}\right]\omega_{M3,B}\ k_{\beta,B}\quad ;\quad \mu^{M2}_{\rho B_\beta} = \sigma^{photo}_{M2,B}\ \omega_{M2,B}\ k_{\beta,B} \quad (29)$$

if $E_{M3} < E_{A_\alpha} < E_{M2}$

$$\sigma^{photo}_{Mj,B} = \frac{S_{Mj}-1}{\Pi^j_{i=1}(S_{Mi})}\sigma_{T,B}\ \text{ for } j\in[4,5]\ ;\ \sigma^{photo}_{M3,B} = \frac{S_{M3}-1}{(S_{M3})}\sigma_{T,B} \quad (30)$$

$$\mu^{M5}_{\rho B_\beta} = \left[(f_{M34}f_{M45}+f_{M35})\sigma^{photo}_{M3,B} + f_{M45}\ \sigma^{photo}_{M4,B} + \sigma^{photo}_{M5,B}\right]\omega_{M5,B}\ k_{\beta,B} \quad (31)$$

$$\mu^{M4}_{\rho B_\beta} = \left[f_{M34}\ \sigma^{photo}_{M3,B} + \sigma^{photo}_{M4,B}\right]\omega_{M4,B}\ k_{\beta,B}\ ;\ \mu^{M3}_{\rho B_\beta} = \sigma^{photo}_{M3,B}\ \omega_{M3,B}\ k_{\beta,B} \quad (32)$$

if $E_{M4} < E_{A_\alpha} < E_{M3}$

$$\sigma^{photo}_{M5,B} = \frac{S_{M5}-1}{(S_{M4}S_{M5})}\ \sigma_{T,B}\ ;\ \sigma^{photo}_{M4,B} = \frac{S_{M4}-1}{S_{M4}}\ \sigma_{T,B} \quad (33)$$

$$\mu^{M4}_{\rho B_\beta} = \sigma^{photo}_{M4,B}\ \omega_{M4,B}\ k_{\beta,B} \quad (34)$$

$$\mu^{M5}_{\rho B_\beta} = \left[\sigma^{photo}_{M3,B} + f_{M45}\ \sigma^{photo}_{M4,B} + \sigma^{photo}_{M5,B}\right]\omega_{M5,B}\ k_{\beta,B} \quad (35)$$

if $E_{M5} < E_{A_\alpha} < E_{M4}$

$$\sigma^{photo}_{M5,B} = \frac{S_{M5}-1}{S_{M5}}\ \sigma_{T,B} \quad (36)$$

$$\mu^{M5}_{\rho B_\beta} = \sigma^{photo}_{M5,B}\ \omega_{M5,B}\ k_{\beta,B} \quad (37)$$

3.2.2 Secondary fluorescence production and survival

Using the definitions of the primary A_α X-rays production density function $\mathscr{P}^X_{A_\alpha}(E(x_1))$ and the conversion probability $\mathscr{R}^\eta_{B_\beta}(A_\alpha)$, the differential density function describing the conversion of primary A_α X-rays produced at a penetration depth x_1 into secondary fluorescence B_β X-rays at volume element dV, which reach the target surface, $dX_{B_\beta A_\alpha}(x_1)$, defined in eq(**??**), may be rewritten as:

$$dX_{B_\beta}(A_\alpha;x_1) = \sigma^X_{A_\alpha,Z_i}(E(x_1))\,f_A\ f_B\ T_{B_\beta}(x_1,r,\theta)\left[\frac{\mu^\eta_{\rho B_\beta}(A_\alpha)}{\mu_{A_\alpha}}\right]_{dV}\mathscr{Q}_{A_\alpha}(x_1,r)\ dV \quad (38)$$

In order to obtain the density function for secondary B_β X-rays emerging from the target surface towards the detector, due to secondary emission induced by primary A_α X-rays emitted at penetration depth x_1 it is necessary to integrate eq(**??**) over the whole target volume, and we can use this step to define the corresponding specific density function, $\chi_{B_\beta A_\alpha}(x_1)$ by dividing by f_B, the result obtained is:

$$\chi_{B_\beta A_\alpha}(x_1) = \sigma^X_{A_\alpha,Z_i}(E(x_1))\,f_A\left(\int_{V_{target}} T_{B_\beta}(x_1,r,\theta)\ \frac{\mu^\eta_{\rho B_\beta}(A_\alpha)}{\mu_{A_\alpha}}\ \mathscr{Q}_{A_\alpha}(x_1,r)\ dV\right) \quad (39)$$

The integral in eq(**??**) represents the fraction of primary A_α X-rays that may be converted to secondary B_β X-rays, and if that happens will survive up to the point of reaching the target surface.

3.2.3 The $\mathscr{Q}_{B_\beta A_\alpha}(x_1)$ function and SFC equivalent thickness

In order to analyse properly eq(**??**), it is important to focus into the differential under the integral:

$$d\mathscr{Q}_{B_\beta A_\alpha}(x_1,r) = T_{B_\beta}(x_1,r,\theta)\ \frac{\mu^\eta_{\rho B_\beta}(A_\alpha)}{\mu_{A_\alpha}}\ \mathscr{Q}_{A_\alpha}(x_1,r)\ dV \quad (40)$$

This is the differential cross-section for a primary A_α X-ray produced at the penetration depth x_1 to be absorbed at a distance r from x_1 and converted into a secondary B_β X-ray that reaches the target surface along a trajectory that leads to the X-ray detector.

Although it looks simple, there are a few details, including theoretical ones, which are worth taking into account carefully.

The most critical term, even if it may not seem so, is the detailed description of the absorption of A_α X-rays in the differential volume. Using spherical coordinates, there are two main components in this process. A geometrical one that relates to the angular description, that leads to a term in the angular variables, namely $r^2 sin(\theta)\ d\theta\ d\phi$, and a second term related to the ionization process itself.

Since X-rays vanish when interacting with atoms to produce an ionization process, as oposed to what is observed with ions, which just loose energy but do not vanish, the number of matrix atoms ionized is proportional to the number of absorbed X-rays.

Considering a small slab of thickness $\Delta r \to dr$ this results in the following expression for the number of absorbed A_α X-rays, $N^{abs}_{X(A_\alpha)}$, using a first order Taylor series approximation:

$$\begin{aligned}N^{abs}_{X(A_\alpha)}(\Delta r) &= N_{X(A_\alpha)}(0)\left(1-e^{-\mu_{A_\alpha}\Delta r}\right) \to \\ &\to N_{X(A_\alpha)}(0)\frac{\partial}{\partial r}\left(1-e^{-\mu_{A_\alpha} r}\right)\Big|_{r=0} dr = \mu_{A_\alpha}\ N_{X(A_\alpha)}(0)\ dr\end{aligned} \quad (41)$$

$N_{X(A_\alpha)}(0)$ being the number of X-rays reaching the slab. The absorption in volume dV therefore contributes with an overall term given by $\mu_{A_\alpha} r^2 sin(\theta)\ dr\ d\theta\ d\phi$.

Taking into account that this expression makes use of the number of X-rays reaching the slab, a term describing the loss of intensity of A_α X-rays between the emission point x_1 and the absorbing volume dV, must be considered. Therefore, the differential

View Article Online
DOI: 10.1039/D4JA00463A

cross-section for A_α X-ray to be absorbed in volume dV at a distance r away from the emission point x_1 is:

$$\mathscr{Q}_{A_\alpha}(x_1,r)\,dV = \frac{\mu_{A_\alpha}}{4\pi r^2}\cdot e^{-\mu_{A_\alpha} r} r^2 sin(\theta)\ dr\ d\theta\ d\phi \tag{42}$$

The remaining term to be mentioned is the probability that the B_β X-rays emitted in elemental volume dV in the direction of the detector reaches the target surface. Being μ_{B_β} the target mass absorption coefficient and x_1 and r expressed in consistent units, usualy areal mass units, the result is:

$$T_{B_\beta}(x_1,r,\theta) = e^{-\mu_{B_\beta}\frac{x_1\cos(\psi_{inc})+r\cdot\cos\theta}{\cos(\psi_{det})}} \tag{43}$$

Finally, writing the whole term in spherical coordinates, for an homogeneous target (see fig.(**??**)), the result is:

$$d\mathscr{Q}_{B_\beta A_\alpha}(x_1,r) = \frac{\mu_{A_\alpha}}{4\pi r^2}\cdot e^{-\mu_{A_\alpha} r}\cdot e^{-\mu_{B_\beta}\frac{x_1\cos(\psi_{inc})+r\cdot\cos\theta}{\cos(\psi_{det})}}\ \frac{\mu^{\eta}_{\rho B_\beta}(A_\alpha)}{\mu_{A_\alpha}}\ r^2\sin(\theta)\ dr\ d\theta\ d\phi \tag{44}$$

The final expression being therefore:

$$d\mathscr{Q}_{B_\beta A_\alpha}(x_1,r) = \frac{\mu^{\eta}_{\rho B_\beta}(A_\alpha)}{4\pi}\cdot e^{-\mu_{A_\alpha} r}\cdot e^{-\mu_{B_\beta}\frac{x_1\cos(\psi_{inc})+r\cdot\cos(\theta)}{\cos(\psi_{det})}}\ \sin(\theta)\ dr\ d\theta\ d\phi \tag{45}$$

This $d\mathscr{Q}_{B_\beta A_\alpha}(x_1,r)$ differential may be refered to as the secondary fluorescence differential cross-section for the conversion of A_α X-rays in B_β X-rays that emerge from the target in the direction of the detector.

The $\mathscr{Q}_{B_\beta A_\alpha}(x_1)$ function defined as the integral of $d\mathscr{Q}_{B_\beta A_\alpha}(x_1,r)$ over the whole target volume is the secondary fluorescence target yield, emitted in the direction of the detector, originated in the conversion of A_α X-rays in B_β X-rays, and corresponds to the integral in eq(**??**).

Using the fact that $d\mathscr{Q}_{B_\beta A_\alpha}(x_1,r)$ has cylindrical symmetry, the $\mathscr{Q}_{B_\beta A_\alpha}(x_1)$ integral can be imediately integrated in ϕ by taking the x axis as being along the normal to target surface. Notice that the x axis for calculating the integral in eq(**??**) is independent of the definition of x_1 along the ion beam penetration path and therefore the x axis for this calculation can be set freely. The result after integrating over ϕ is:

$$\mathscr{Q}_{B_\beta A_\alpha}(x_1) = \frac{\mu^{\eta}_{\rho B_\beta}(A_\alpha)}{2}\cdot e^{-\mu_{B_\beta}\frac{x_1\cos(\psi_{inc})}{\cos(\psi_{det})}}\iint_V e^{-\left(\mu_{A_\alpha}+\frac{\cos(\theta)}{\cos(\psi_{det})}\mu_{B_\beta}\right)\cdot r}\sin(\theta)\ drd\theta \tag{46}$$

Summing up for all primary A_α X-rays produced at penetration depth x_1 and leading to B_β secondary X-rays, the specific secondary fluorescence correction density function, $\chi_{B_\beta}(x_1)$, can be written as:

$$\chi_{B_\beta}(x_1) = \sum_{\substack{all A_\alpha\\ \text{inducing } B_\beta}} \sigma^X_{A\alpha,Z_i}(E(x_1))\,f_A\ \mathscr{Q}_{B_\beta A_\alpha}(x_1) \tag{47}$$

and added to the equivalent thickness definition, leading to a secondary fluorescence corrected equivalent thickness, $\xi^{sfc}_{eq,B_\beta}(E_p)$, which becomes now dependent not just on the X-ray being detected, but also on the various other X-ray emitters in the target:

$$\xi^{sfc}_{eq,B_\beta}(E_p) = \int_0^{x(E_{out})}\frac{\sigma^X_{j(\beta),Z(B)}(E(x))\cdot T_{j(\beta),Z(B)}(x)\ +\ \chi_{B_\beta}(x)}{\sigma^X_{j(\beta),Z(B)}(E_p)}\ dx \tag{48}$$

4 The $\mathscr{Q}_{B_\beta A_\alpha}(x_1)$ function analytical solution

4.1 First steps for solving the integral analyticaly

Considering that r is small relative to the distance to the detector, so that it is possible to assume that the detection angle ψ_{det} is constant relative to r, eq(**??**) integral can be solved analytically, as long as it can be assumed that the sample is infinite and homogeneous in all planes normal to the surface normal, at least for the fluorescence process. This meaning that the model, may be easily addapted to still be applied to a small inclusion emitting primary X-rays if the particle beam is kept within it, but is not applicable to a case of a small inclusion emitting secondary X-rays due to primary X-rays originated in its surroundings.

In order to obtain the analytical solution, it is important to start by a change of variable, namely by setting:

$$y = \mu_{A_\alpha} + \frac{\cos(\theta)}{\cos(\psi_{det})}\mu_{B_\beta} \Rightarrow \cos(\theta) = (y-\mu_{A_\alpha})\cdot\frac{\cos(\psi_{det})}{\mu_{B_\beta}} \Rightarrow$$
$$\Rightarrow \sin(\theta)d\theta = -\frac{\cos(\psi_{det})}{\mu_{B_\beta}}dy \tag{49}$$

The $\mathscr{Q}_{B_\beta A_\alpha}(x_1)$ expression can then be simplified to:

$$\mathscr{Q}_{B_\beta A_\alpha}(x_1) = \mathscr{A}(x_1)\int_{r_{min}}^{r_{max}}\int_{\mu_{A_\alpha}+\frac{\mu_{B_\beta}}{\cos(\psi_{det})}\cos(\theta_i)}^{\mu_{A_\alpha}+\frac{\mu_{B_\beta}}{\cos(\psi_{det})}\cos(\theta_f)} -e^{-y\cdot r}\ dy\ dr \tag{50}$$

being

$$\mathscr{A}(x_1) = \frac{\mu^{\eta}_{\rho B_\beta}(A_\alpha)\cdot cos(\psi_{det})}{2\cdot\mu_{B_\beta}}\cdot e^{-\mu_{B_\beta}\frac{x_1 cos(\psi_{inc})}{\cos(\psi_{det})}} \tag{51}$$

Calculating the integral in eq(**??**) is better done by separating the full integral in six different cases according to the relations between d and t described in Table **??** (see fig.(**??**) for variables references).

Equation eq(**??**) is thus better written as (i values according to Table **??**):

$$\mathscr{Q}_{B_\beta A_\alpha}(x_1) = \mathscr{A}(x_1)\cdot\sum_i I_i \tag{52}$$

being:

$$I_i = \int_{r_{min,i}}^{r_{max,i}}\ \frac{e^{-y\cdot r}}{r}\ \Bigg|_{\mu_{A_\alpha}+\frac{\mu_{B_\beta}}{\cos(\psi_{det})}\cos(\theta_i)}^{\mu_{A_\alpha}+\frac{\mu_{B_\beta}}{\cos(\psi_{det})}\cos(\theta_f)}\ dr \tag{53}$$

Table 1 Integration limits for r and θ for the various integrals (I_1 to I_6).

	i	$r_{min,i}$	$r_{max,i}$	$\cos\theta_i$	$\cos\theta_f$
$d <= t/2$	1	0	d	1	-1
	2	d	t-d	1	-d/r
	3	t-d	∞	(t-d)/r	-d/r
$d > t/2$	4	0	t-d	1	-1
	5	t-d	d	(t-d)/r	-1
	6	d	∞	(t-d)/r	-d/r

Setting now:

$$g_+ = \mu_{A_\alpha} + \frac{\mu_{B_\beta}}{\cos(\psi_{det})}\quad\text{and}\quad g_- = \mu_{A_\alpha} - \frac{\mu_{B_\beta}}{\cos(\psi_{det})} \tag{54}$$

the first three integrals mentioned above become:

$$I_1 = \int_0^d\ \frac{e^{-y\cdot r}}{r}\ \Bigg|_{g_+}^{g_-}\ dr \tag{55}$$

$$I_2 = \int_d^{t-d}\ \frac{e^{-y\cdot r}}{r}\ \Bigg|_{g_+}^{\mu_{A_\alpha}-\frac{\mu_{B_\beta}\cdot d}{\cos(\psi_{det})\cdot r}}\ dr \tag{56}$$

$$I_3 = \int_{t-d}^{\infty}\ \frac{e^{-y\cdot r}}{r}\ \Bigg|_{\mu_{A_\alpha}+\frac{\mu_{B_\beta}\cdot(t-d)}{\cos(\psi_{det})\cdot r}}^{\mu_{A_\alpha}-\frac{\mu_{B_\beta}\cdot d}{\cos(\psi_{det})\cdot r}}\ dr \tag{57}$$

Expanding these expressions leads to:

$$I_1 = 2\int_0^d\ \frac{e^{-\mu_{A_\alpha}\cdot r}}{r}\ \frac{\left(e^{\frac{\mu_{B_\beta}\cdot r}{\cos(\psi_{det})}} - e^{-\frac{\mu_{B_\beta}\cdot r}{\cos(\psi_{det})}}\right)}{2}\ dr$$
$$= 2\int_0^d \frac{e^{-\mu_{A_\alpha}\cdot r}}{r}\cdot\sinh\left(\frac{\mu_{B_\beta}\cdot r}{\cos(\psi_{det})}\right)\ dr \tag{58}$$

$$I_2 = \int_d^{t-d}\ \frac{e^{-\mu_{A_\alpha}\cdot r}}{r}\ \left(e^{\frac{\mu_{B_\beta}\cdot d}{\cos(\psi_{det})}} - e^{-\frac{\mu_{B_\beta}\cdot r}{\cos(\psi_{det})}}\right)\ dr$$
$$= e^{\frac{\mu_{B_\beta}\cdot d}{\cos(\psi_{det})}}\int_d^{t-d}\ \frac{e^{-\mu_{A_\alpha}\cdot r}}{r}dr - \int_d^{t-d}\ \frac{e^{-\left(\mu_{A_\alpha}+\frac{\mu_{B_\beta}}{\cos(\psi_{det})}\right)\cdot r}}{r}dr \tag{59}$$

$$I_3 = \int_{t-d}^{\infty}\ \frac{e^{-\mu_{A_\alpha}\cdot r}}{r}\ \left(e^{\frac{\mu_{B_\beta}\cdot d}{\cos(\psi_{det})}} - e^{-\frac{\mu_{B_\beta}\cdot(t-d)}{\cos(\psi_{det})}}\right)\ dr$$
$$= e^{\frac{\mu_{B_\beta}\cdot d}{\cos(\psi_{det})}}\left(1 - e^{-\frac{\mu_{B_\beta}\cdot t}{\cos(\psi_{det})}}\right)\int_{t-d}^{\infty}\ \frac{e^{-\mu_{A_\alpha}\cdot r}}{r}dr \tag{60}$$

Now, Gradshteyn[?] states:

$$\int\frac{1}{x}e^{ax}\sinh(bx)dx = \frac{1}{2}\{E_i[(a+b)x] - E_i[(a-b)x]\}\ \text{for}\ a^2\neq b^2 \tag{61}$$

Both Gradshteyn[?] and Abramowicz[?] define the exponential integral as:

$$E_i(x) = -\lim_{\varepsilon\longrightarrow 0^+}\left[\int_{-x}^{-\varepsilon}\frac{e^{-t}}{t}dt + \int_{\varepsilon}^{\infty}\frac{e^{-t}}{t}dt\right]\quad (x>0) \tag{62}$$

Gradshteyn further sets for negative values of x : $E_i(x) = -\int_{-x}^{\infty}\frac{e^{-t}}{t}dt\quad (x<0)$, while Abramowicz[?] defines the exponential integral of order 1 for positive values of the variable as:

$$E_1(x) = \int_x^{\infty}\frac{e^{-t}}{t}dt\ \ \text{for}\ \ (x>0) \tag{63}$$

Leading to the relation:

$$E_i(x) \underset{x<0}{=} -\int_{|x|}^{\infty}\frac{e^{-t}}{t}dt = -\int_{y>0}^{\infty}\frac{e^{-t}}{t}dt = -E_1(y) = -E_1(-x) \tag{64}$$

These Abramowicz definitions having $x\in\,]0,\infty[$ will be used for the remaining of this work.

The exponential integral and the exponential integral of order 1 may still be presented as series of powers as:

$$E_i(y) = \gamma + ln(y) + \sum_{n=1}^{\infty}\frac{y^n}{n\cdot n!}\ \ ;\ \ E_1(y) = -\gamma - ln(y) - \sum_{n=1}^{\infty}\frac{(-1)^n\cdot y^n}{n\cdot n!} \tag{65}$$

View Article Online
DOI: 10.1039/D4JA00463A

where $\gamma = 0.57721156649....$ is Euler's constant.

Now in eq(**??**) the signal of the constants in the exponential and $\sinh()$ function are well defined since both the mass absoption coefficients and the distances are positive.

Before applying eq(**??**) to eq(**??**) it is still important to obtain a few additional expressions.

Assuming $a > 0$, $b > 0$ and $x > 0$, from eq(**??**) using Abramowicz nomenclature, it is important to note that:

$$\int \frac{1}{x} e^{-ax} \sinh(bx) dx = \frac{1}{2} \{E_i[-(a-b)x] - E_i[-(a+b)x]\}$$

$$= \frac{1}{2} \{E_1[(a+b)x] - E_1[(a-b)x]\} \quad if \;\; a > b \tag{66}$$

$$= \frac{1}{2} \{E_1[(a+b)x] + E_i[|a-b|x]\} \quad if \;\; a < b \tag{67}$$

If $a = b$ Gradshteyn in its equation 2.484.6[?] further states:

$$\int \frac{1}{x} e^{-ax} \sinh(bx) dx = \frac{1}{2} [ln(x) - E_i(-2ax)]$$

that converting to Abramowicz nomenclature becomes:

$$\int \frac{1}{x} e^{-ax} \sinh(bx) dx = \frac{1}{2} [ln(x) + E_1(2ax)] \quad if \;\; a = b \tag{68}$$

Before applying these expressions to eq(**??**) and other integrals, it is important to check the case where $x \longrightarrow 0$, since in this condition, $ln(x)$, $E_i()$ and $E_1()$ are divergent. The differences limits are:

$$\lim_{x \longrightarrow 0} \Big(E_1[(a+b)x] - E_1[(a-b)x] \Big) = \lim_{x \longrightarrow 0} \Bigg(-\gamma - ln[(a+b)x] - \sum_{n=1}^{\infty} \frac{(-1)^n \cdot [(a+b)x]^n}{n \cdot n!} +$$

$$+ \gamma + ln[(a-b)x] + \sum_{n=1}^{\infty} \frac{(-1)^n \cdot [(a-b)x]^n}{n \cdot n!} \Bigg)$$

$$= \lim_{x \longrightarrow 0} \left[ln\left(\frac{a-b}{a+b}\right) + \sum_{n=1}^{\infty} \frac{(-1)^n [(a-b)x]^n}{nn!} - \sum_{n=1}^{\infty} \frac{(-1)^n [(a+b)x]^n}{nn!} \right]$$

$$= -ln\left(\frac{a+b}{a-b}\right) \quad if \;\; a > b \tag{69}$$

$$\lim_{x \longrightarrow 0} \Big(E_1[(a+b)x] + E_i[|a-b|x] \Big) = \lim_{x \longrightarrow 0} \Bigg(-\gamma - ln[(a+b)x] - \sum_{n=1}^{\infty} \frac{(-1)^n \cdot [(a+b)x]^n}{n \cdot n!} +$$

$$+ \gamma + ln[|a-b|x] + \sum_{n=1}^{\infty} \frac{[|a-b|x]^n}{n \cdot n!} \Bigg)$$

$$= \lim_{x \longrightarrow 0} \left[ln\left(\frac{|a-b|}{a+b}\right) + \sum_{n=1}^{\infty} \frac{[|a-b|x]^n}{n \cdot n!} - \sum_{n=1}^{\infty} \frac{(-1)^n [(a+b)x]^n}{n \cdot n!} \right]$$

$$= -ln\left(\frac{a+b}{|a-b|}\right) \quad if \;\; a < b \tag{70}$$

$$\lim_{x \longrightarrow 0} \Big(E_1(2ax) + ln(x) \Big) = \lim_{x \longrightarrow 0} \left(-\gamma - ln(2ax) - \sum_{n=1}^{\infty} \frac{(-1)^n \cdot (2ax)^n}{n \cdot n!} + ln(x) \right)$$

$$= \lim_{x \longrightarrow 0} \left[-\gamma - ln(2a) - \sum_{n=1}^{\infty} \frac{(-1)^n \cdot (2ax)^n}{n \cdot n!} \right]$$

$$= -[\gamma + ln(2a)] \quad if \;\; a = b \tag{71}$$

Setting $a = \mu_{A_\alpha}$ and $b = \frac{\mu_{B_\beta}}{\cos(\psi_{det})}$, and applying these to the definitive integral I_1 the result is:

$$\int_0^d \frac{1}{x} e^{-ax} \sinh(bx) dx = \frac{1}{2} \left\{E_1[(a+b)d] - E_1[(a-b)d] + ln\left(\frac{a+b}{(a-b)}\right)\right\} \quad if \;\; a > b \tag{72}$$

$$= \frac{1}{2} \left\{E_1[(a+b)d] + E_i[|a-b|d] + ln\left(\frac{a+b}{|a-b|}\right)\right\} \quad if \;\; a < b \tag{73}$$

$$= \frac{1}{2} [E_1(2ad) + ln(2ad) + \gamma] \quad if \;\; a = b \tag{74}$$

It is important to realise that, from the equations above, it results for all these cases:

$$\lim_{d \to 0} \int_0^d \frac{1}{x} e^{-ax} \sinh(bx) dx = 0 \tag{75}$$

These results can be written in a more condensed and physically interesting form, namelly:

$$I_1 = E_1(g_+ \cdot d) - E_1(g_- \cdot d) + ln\left(\frac{g_+}{g_-}\right) \quad if \;\; g_- > 0 \tag{76}$$

$$I_1 = E_1(g_+ \cdot d) + E_i(|g_-| \cdot d) + ln\left(\frac{g_+}{|g_-|}\right) \quad if \;\; g_- < 0 \tag{77}$$

$$I_1 = E_1(2\mu_{A_\alpha} \cdot d) + ln(2\mu_{A_\alpha} d) + \gamma \quad if \;\; g_- = 0 \tag{78}$$

Addressing the calculation of the definitive integral I_2, eqs(**??** to **??**) are not applicable to eq(**??**) and the definition eqs(**??** to **??**) must be used directly. Setting $\zeta > 0$ and $\eta > 0$ and $y = at$ the result is:

$$\int_\eta^\zeta \frac{e^{-at}}{t} dt = \int_\eta^\infty \frac{e^{-at}}{t} dt - \int_\zeta^\infty \frac{e^{-at}}{t} dt = \int_{a\eta}^\infty \frac{e^{-y}}{y} dy - \int_{a\zeta}^\infty \frac{e^{-y}}{y} dy =$$

$$= E_1(a\eta) - E_1(a\zeta) \;\; \text{for} \;\; (a > 0) \tag{79}$$

$$= E_i(|a|\zeta) - E_i(|a|\eta) \;\; \text{for} \;\; (a < 0) \tag{80}$$

Applying this to eq(**??**) the result is:

$$I_2 = e^{\frac{\mu_{B_\beta} \cdot d}{\cos(\psi_{det})}} \int_d^{t-d} \frac{e^{-\mu_{A_\alpha} \cdot r}}{r} dr - \int_d^{t-d} \frac{e^{-\left(\mu_{A_\alpha} + \frac{\mu_{B_\beta}}{\cos(\psi_{det})}\right) \cdot r}}{r} dr$$

$$= e^{\frac{\mu_{B_\beta} \cdot d}{\cos(\psi_{det})}} \Big(E_1(\mu_{A_\alpha} \cdot d) - E_1[\mu_{A_\alpha} \cdot (t-d)] \Big) -$$

$$- \left(E_1\left[\left(\mu_{A_\alpha} + \frac{\mu_{B_\beta}}{\cos(\psi_{det})}\right) \cdot d \right] - E_1\left[\left(\mu_{A_\alpha} + \frac{\mu_{B_\beta}}{\cos(\psi_{det})}\right) \cdot (t-d) \right] \right)$$

$$I_2 = e^{\frac{\mu_{B_\beta} \cdot d}{\cos(\psi_{det})}} \Big[E_1(\mu_{A_\alpha} \cdot d) - E_1[\mu_{A_\alpha} \cdot (t-d)] \Big] - \Big[E_1(g_+ \cdot d) - E_1[g_+ \cdot (t-d)] \Big] \tag{81}$$

4.2 Infinite thickness targets

In the case of thick targets, $t = \infty$ and only I_1 and I_2 apply. Adding eqs.(**??** to **??**) and (**??**) provides:

$$I_1 + I_2^\infty = e^{\frac{\mu_{B_\beta} \cdot d}{\cos(\psi_{det})}} E_1(\mu_{A_\alpha} \cdot d) - E_1(g_- \cdot d) + ln\left(\frac{g_+}{g_-}\right) \quad for \;\; g_- > 0 \tag{82}$$

$$I_1 + I_2^\infty = e^{\frac{\mu_{B_\beta} \cdot d}{\cos(\psi_{det})}} E_1(\mu_{A_\alpha} \cdot d) + E_i(|g_-| \cdot d) + ln\left(\frac{g_+}{|g_-|}\right) \quad for \;\; g_- < 0 \tag{83}$$

$$I_1 + I_2^\infty = E_1(2\mu_{A_\alpha} \cdot d) + e^{\frac{\mu_{B_\beta} \cdot d}{\cos(\psi_{det})}} E_1(\mu_{A_\alpha} \cdot d) - E_1(g_+ \cdot d) + ln(2\mu_{A_\alpha} d) + \gamma$$

$$= e^{\frac{\mu_{B_\beta} \cdot d}{\cos(\psi_{det})}} E_1(\mu_{A_\alpha} \cdot d) + ln(2\mu_{A_\alpha} d) + \gamma \quad for \;\; g_- = 0 \Rightarrow g_+ = 2\mu_{A_\alpha} \tag{84}$$

The computation implementation of these results must take into account that for very small values of the argument, the exponential intergral diverges due to the term in $ln(x)$ in eqs.(**??**). Still, in the case of small values of d (x_1 still close to target surface) no problems are faced since the results are:

$$\lim_{d \to 0} (I_1 + I_2^\infty) = \lim_{d \to 0} \left[e^{\frac{\mu_{B_\beta} \cdot d}{\cos(\psi_{det})}} \Big(-\gamma - ln(\mu_{A_\alpha} \cdot d) \Big) - \Big(-\gamma - ln(g_- \cdot d) \Big) + ln\left(\frac{g_+}{g_-}\right) \right]$$

$$= \lim_{d \to 0} \left[\left(1 - e^{\frac{\mu_{B_\beta} \cdot d}{\cos(\psi_{det})}}\right) \gamma - e^{\frac{\mu_{B_\beta} \cdot d}{\cos(\psi_{det})}} [ln(\mu_{A_\alpha}) + ln(d)] + ln(g_-) + ln(d) + ln\left(\frac{g_+}{g_-}\right) \right]$$

$$= ln\left(\frac{g_+}{\mu_{A_\alpha}}\right) \quad for \;\; g_- > 0 \tag{85}$$

$$\lim_{d \to 0} (I_1 + I_2^\infty) = \lim_{d \to 0} \left[e^{\frac{\mu_{B_\beta} \cdot d}{\cos(\psi_{det})}} \Big(-\gamma - ln(\mu_{A_\alpha} \cdot d) \Big) + \Big(\gamma + ln(|g_-| \cdot d) \Big) + ln\left(\frac{g_+}{|g_-|}\right) \right]$$

$$= \lim_{d \to 0} \left[\left(1 - e^{\frac{\mu_{B_\beta} \cdot d}{\cos(\psi_{det})}}\right) \gamma - e^{\frac{\mu_{B_\beta} \cdot d}{\cos(\psi_{det})}} [ln(\mu_{A_\alpha}) + ln(d)] + ln(|g_-|) + ln(d) + ln\left(\frac{g_+}{|g_-|}\right) \right]$$

$$= ln\left(\frac{g_+}{\mu_{A_\alpha}}\right) \quad for \;\; g_- < 0$$

$$\lim_{d \to 0} (I_1 + I_2^\infty) = \lim_{d \to 0} \left[e^{\frac{\mu_{B_\beta} \cdot d}{\cos(\psi_{det})}} \Big(-\gamma - ln(\mu_{A_\alpha} \cdot d) \Big) + ln(2\mu_{A_\alpha} \cdot d) + \gamma \right] \tag{86}$$

$$= ln(2) \quad for \;\; g_- = 0 \tag{87}$$

Before proceeding to deal with half-thick targets, it is still important to check the theoretical possibility that d is not too small but either $|g_-|$ is too small but not enough to make the product $|g_-| \cdot d$ too small, or the mass absorption coefficient of the A_α X-rays is so small that the product $\mu_{A_\alpha} \cdot d \to 0$. In all these cases numerical calculation problems emerge linked to eqs(**??**) to (**??**). Besides, the problematic conditions in $|g_-|$ may also combine with those on μ_{A_α} and therefore all cases must be addressed carefully.

Taking into account the power series expansions in eqs.(**??**) the results for $|g_-| \to 0$ while the product $|g_-| \cdot d$ is not, are:

$$\lim_{|g_-| \longrightarrow 0^+} (I_1 + I_2^\infty) = \lim_{|g_-| \longrightarrow 0^-} (I_1 + I_2^\infty) = e^{\frac{\mu_{B_\beta} \cdot d}{\cos(\psi_{det})}} E_1(\mu_{A_\alpha} \cdot d) + \gamma + log(g_+ \cdot d) \tag{88}$$

As could be expected this expression is identical to that of eq(**??**) since in the limit $g_+ = 2\mu_{A_\alpha}$. In the case where $\mu_{A_\alpha} \cdot d \to 0$, two conditions can be found, namely, $|g_-| \to 0$, or not so and $g_- < 0$. In the first of these, eq(**??**) limit is $ln(2)$. In the second case, it is necessary to establish an *ad-hoc* cut-off, say $\mathscr{C}_{off}$ corresponding to a 95% intensity decrease of A_α X−rays, which results on eqs(**??**) and (**??**) to become:

View Article Online
DOI: 10.1039/D4JA00463A

$$\begin{aligned}\lim_{\mu_{A_\alpha}\longrightarrow 0} I_1 &= \int_0^d \frac{1}{r}\left(e^{\frac{\mu_{B_\beta}\cdot r}{\cos(\psi_{det})}} - e^{-\frac{\mu_{B_\beta}\cdot r}{\cos(\psi_{det})}}\right) dr \\ &= \int_0^d \frac{e^{br}}{r}\, dr - \int_0^d \frac{e^{-br}}{r}\, dr = -\left(\int_{-d}^0 \frac{e^{-b\eta}}{\eta}\, d\eta + \int_0^d \frac{e^{-br}}{r}\, dr\right) \\ &= -\lim_{\varepsilon\longrightarrow 0}\left(\int_{-d}^\infty \frac{e^{-b\eta}}{\eta}\, d\eta - \int_\varepsilon^\infty \frac{e^{-b\eta}}{\eta}\, d\eta + \int_\varepsilon^d \frac{e^{-br}}{r}\, dr\right) \\ &= -\lim_{\varepsilon\longrightarrow 0}\Big(-E_i(bd) - E_i(b\varepsilon) + E_1(b\varepsilon) - E_1(bd)\Big) \\ &= E_1(bd) + E_i(bd) \end{aligned} \tag{89}$$

$$\begin{aligned}\lim_{\mu_{A_\alpha}\longrightarrow 0} I_2^{\mathscr{C}_{off}} &= \int_d^{\mathscr{C}_{off}} \frac{1}{r}\left(e^{\frac{\mu_{B_\beta}\cdot d}{\cos(\psi_{det})}} - e^{-\frac{\mu_{B_\beta}\cdot r}{\cos(\psi_{det})}}\right) dr \\ &= e^{bd}\int_d^{\mathscr{C}_{off}} \frac{1}{r}\, dr - \int_d^{\mathscr{C}_{off}} \frac{e^{-br}}{r} dr \\ &= e^{bd}\cdot ln\left(\frac{\mathscr{C}_{off}}{d}\right) - E_1(bd) + E_1(b\,\mathscr{C}_{off}) \end{aligned} \tag{90}$$

which summing up provides :

$$\lim_{\mu_{A_\alpha}\longrightarrow 0} I_1 + I_2^{\mathscr{C}_{off}} = E_i(b\cdot d) + e^{b\cdot d}\cdot ln\left(\frac{\mathscr{C}_{off}}{d}\right) + E_1(b\cdot\mathscr{C}_{off}) \text{ being } b = \frac{\mu_{B_\beta}}{\cos(\psi_{det})} \tag{91}$$

If in this case $d \to 0$ this equation is also not valid. Using the power series expansions leads to:

$$\lim_{\mu_{A_\alpha}\longrightarrow 0} I_1 + I_2^{\mathscr{C}_{off}} = \gamma + E_1(b\cdot\mathscr{C}_{off}) + ln(b\cdot\mathscr{C}_{off}) \tag{92}$$

4.3 Homogeneous half-thick targets

4.3.1 Primary X-rays emitted before half-layer depth

In the general case of half-thick targets, all the the six integrals must be calculated. As can be seen from table **??**, the six integrals are separated in two distinct cases. Integrals I_1 to I_3 provide the results for the situation where the point x_1 exist at a distance to the target surface less than half of the target thickness, and integrals I_4 to I_6 provide results for the situation where this is not so and therefore $d > t/2$.

In the case of I_3, eq(**??**) should be applied directly to eq(**??**), the result being:

$$\begin{aligned} I_3 &= e^{\frac{\mu_{B_\beta}\cdot d}{\cos(\psi_{det})}}\left(1 - e^{-\frac{\mu_{B_\beta}\cdot t}{\cos(\psi_{det})}}\right)\int_{t-d}^\infty \frac{e^{-\mu_{A_\alpha}\cdot r}}{r} dr \\ &= e^{\frac{\mu_{B_\beta}\cdot d}{\cos(\psi_{det})}}\left(1 - e^{-\frac{\mu_{B_\beta}\cdot t}{\cos(\psi_{det})}}\right) E_1[\mu_{A_\alpha}\cdot(t-d)] \end{aligned} \tag{93}$$

therefore, setting $b = \frac{\mu_{B_\beta}}{\cos(\psi_{det})}$, the result for $I_2 + I_3$ is:

$$I_2 + I_3 = e^{b\cdot d}E_1(\mu_{A_\alpha}\cdot d) - e^{-b\cdot(t-d)}E_1[\mu_{A_\alpha}\cdot(t-d)] - \Big[E_1(g_+\cdot d) - E_1[g_+\cdot(t-d)]\Big] \tag{94}$$

For the homogeneous *half-thick* target and $d <= t/2$ the sum of the I_1, I_2 and I_3 results in:

$$\begin{aligned} I_1 + I_2 + I_3 &= E_1[g_+\cdot(t-d)] - E_1(g_-\cdot d) + ln\left(\frac{g_+}{g_-}\right) + \\ &+ e^{b\cdot d}E_1(\mu_{A_\alpha}\cdot d) - e^{-b\cdot(t-d)}E_1[\mu_{A_\alpha}\cdot(t-d)] \qquad if \;\; g_- > 0 \end{aligned} \tag{95}$$

$$\begin{aligned} I_1 + I_2 + I_3 &= E_1[g_+\cdot(t-d)] + E_i(|g_-|\cdot d) + ln\left(\frac{g_+}{|g_-|}\right) + \\ &+ e^{b\cdot d}E_1(\mu_{A_\alpha}\cdot d) - e^{-b\cdot(t-d)}E_1[\mu_{A_\alpha}\cdot(t-d)] \qquad if \;\; g_- < 0 \end{aligned} \tag{96}$$

$$\begin{aligned} I_1 + I_2 + I_3 &= E_1(2\mu_{A_\alpha}\cdot d) + e^{b\cdot d}E_1(\mu_{A_\alpha}\cdot d) + ln(2\mu_{A_\alpha}d) + \gamma - \\ &- e^{-b\cdot(t-d)}E_1[\mu_{A_\alpha}\cdot(t-d)] - \Big[E_1(g_+\cdot d) - E_1[g_+\cdot(t-d)]\Big] \end{aligned}$$

and since $g_- = 0 \Rightarrow g_+ = 2\mu_{A_\alpha}$,

$$\begin{aligned} I_1 + I_2 + I_3 &= E_1[2\mu_{A_\alpha}\cdot(t-d)] + ln(2\mu_{A_\alpha}d) + \\ &+ \gamma + e^{b\cdot d}E_1(\mu_{A_\alpha}\cdot d) - e^{-b\cdot(t-d)}E_1[\mu_{A_\alpha}\cdot(t-d)] \; if \; g_- = 0 \end{aligned} \tag{97}$$

In this case, when $d \to 0$ the result for all three possibilities is the same, namely:

$$I_1 + I_2 + I_3 = E_1(g_+\cdot t) + ln\left(\frac{g_+}{\mu_{A_\alpha}}\right) - e^{-b\cdot t}E_1(\mu_{A_\alpha}\cdot t) \tag{98}$$

In what concernes other extreme cases, as in the previous subsection, we may find $\mu_{A_\alpha} \to 0$ while d is not too small. Once again we can have two different conditions for this. In the case when $|g_-| \to 0$, the limit of the sums is 0 because if $\mu_{A_\alpha} \to 0$ and $|g_-| \to 0$ then $b \to 0$. If it is instead $g_- < 0$, then b is no longer a vanishing value and a cut-off must be used to calculate the I_3 integral and $(t-d)$ must replace the cut-off in eq(**??**), leading to the result:

$$\begin{aligned} \lim_{\substack{\mu_{A_\alpha}\longrightarrow 0\\ g_-<0,d>0}} (I_1 + I_2 + I_3) &= E_i(b\cdot d) + E_1[b\cdot(t-d)] + \\ &+ e^{b\cdot d}\cdot ln\left(\frac{\mathscr{C}_{off}}{d}\right) - e^{-b\cdot(t-d)}\, ln\left(\frac{\mathscr{C}_{off}}{t-d}\right) \end{aligned} \tag{99}$$

If now both $d \to 0$ and $\mu_{A_\alpha} \to 0$ eq(**??**) must be used to calculate the limit and the result is:

$$\lim_{\substack{\mu_{A_\alpha}\to 0\\ d\to 0}} (I_1 + I_2 + I_3) = E_1(b\cdot t) + \gamma + ln(b\cdot\mathscr{C}_{off}) - e^{-b\cdot t}\, ln\left(\frac{\mathscr{C}_{off}}{t}\right) \tag{100}$$

4.3.2 Primary X-rays emitted after half-layer depth

Since the sum of I_1 to I_3 is only valid for $d <= t/2$, when the contrary is true, meaning when $d > t/2$, the sum of integrals I_4 to I_6 applies.

Based on table **??** these are:

$$I_4 = \int_0^{t-d} \frac{e^{-y\cdot r}}{r}\Bigg|_{g_+}^{g_-} dr \quad ; \quad I_5 = \int_{t-d}^d \frac{e^{-y\cdot r}}{r}\Bigg|_{\mu_{A_\alpha} + \frac{\mu_{B_\beta}\cdot(t-d)}{\cos(\psi_{det})\cdot r}}^{g_-} dr \text{ and}$$

$$I_6 = \int_d^\infty \frac{e^{-y\cdot r}}{r}\Bigg|_{\mu_{A_\alpha} + \frac{\mu_{B_\beta}\cdot(t-d)}{\cos(\psi_{det})\cdot r}}^{\mu_{A_\alpha} - \frac{\mu_{B_\beta}\cdot d}{\cos(\psi_{det})\cdot r}} dr \tag{101}$$

In the case of I_4 given the formal identity to I_1 once d is replaced by $(t-d)$, the result is:

$$I_4 = E_1[g_+\cdot(t-d)] - E_1[g_-\cdot(t-d)] + ln\left(\frac{g_+}{g_-}\right) \qquad if \;\; g_- > 0 \tag{102}$$

$$I_4 = E_1[g_+\cdot(t-d)] + E_i[|g_-|\cdot(t-d)] + ln\left(\frac{g_+}{|g_-|}\right) \qquad if \;\; g_- < 0 \tag{103}$$

$$I_4 = E_1[2\mu_{A_\alpha}\cdot(t-d)] + ln[2\mu_{A_\alpha}(t-d)] + \gamma \qquad if \;\; g_- = 0 \tag{104}$$

In the case of I_5, expanding the expression in eq(**??**) provides:

$$\begin{aligned} I_5 &= \int_{t-d}^d \frac{e^{-\mu_{A_\alpha}\cdot r}}{r}\left(e^{\frac{\mu_{B_\beta}\cdot r}{\cos(\psi_{det})}} - e^{-\frac{\mu_{B_\beta}\cdot(t-d)}{\cos(\psi_{det})}}\right) dr \\ &= \int_{t-d}^d \frac{e^{-g_-\cdot r}}{r} dr - e^{-\frac{\mu_{B_\beta}\cdot(t-d)}{\cos(\psi_{det})}}\int_{t-d}^d \frac{e^{-\mu_{A_\alpha}\cdot r}}{r} dr \end{aligned} \tag{105}$$

Taking into account eqs.(**??**) and (**??**) three results are possible for I_5, namely:

$$\begin{aligned} I_5 &= E_1[g_-\cdot(t-d)] - E_1(g_-\cdot d) - \\ &- e^{-\frac{\mu_{B_\beta}\cdot(t-d)}{\cos(\psi_{det})}}\Big(E_1[\mu_{A_\alpha}\cdot(t-d)] - E_1(\mu_{A_\alpha}\cdot d)\Big) \quad if \;\; g_- > 0 \end{aligned} \tag{106}$$

$$\begin{aligned} I_5 &= E_i(|g_-|\cdot d) - E_i[|g_-|\cdot(t-d)] - \\ &- e^{-\frac{\mu_{B_\beta}\cdot(t-d)}{\cos(\psi_{det})}}\Big(E_1[\mu_{A_\alpha}\cdot(t-d)] - E_1(\mu_{A_\alpha}\cdot d)\Big) \quad if \;\; g_- < 0 \end{aligned} \tag{107}$$

$$\begin{aligned} I_5 &= ln\left(\frac{d}{t-d}\right) - \\ &- e^{-\frac{\mu_{B_\beta}\cdot(t-d)}{\cos(\psi_{det})}}\Big(E_1[\mu_{A_\alpha}\cdot(t-d)] - E_1(\mu_{A_\alpha}\cdot d)\Big) \qquad if \;\; g_- = 0 \end{aligned} \tag{108}$$

In the case of I_6 the result is:

$$\begin{aligned} I_6 &= \int_d^\infty \frac{e^{-\mu_{A_\alpha}\cdot r}}{r}\left(e^{\frac{\mu_{B_\beta}\cdot d}{\cos(\psi_{det})}} - e^{-\frac{\mu_{B_\beta}\cdot(t-d)}{\cos(\psi_{det})}}\right) dr \\ &= e^{\frac{\mu_{B_\beta}\cdot d}{\cos(\psi_{det})}}\left(1 - e^{-\frac{\mu_{B_\beta}\cdot t}{\cos(\psi_{det})}}\right)\int_d^\infty \frac{e^{-\mu_{A_\alpha}\cdot r}}{r} dr \\ &= e^{\frac{\mu_{B_\beta}\cdot d}{\cos(\psi_{det})}}\left(1 - e^{-\frac{\mu_{B_\beta}\cdot t}{\cos(\psi_{det})}}\right) E_1(\mu_{A_\alpha}\cdot d) \end{aligned} \tag{109}$$

Adding I_4, I_5 and I_6 the results are now:

$$\begin{aligned} I_4 + I_5 + I_6 &= E_1[g_+\cdot(t-d)] - E_1(g_-\cdot d) + ln\left(\frac{g_+}{g_-}\right) + \\ &+ e^{\frac{\mu_{B_\beta}\cdot d}{\cos(\psi_{det})}} E_1(\mu_{A_\alpha}\cdot d) - e^{-\frac{\mu_{B_\beta}\cdot(t-d)}{\cos(\psi_{det})}} E_1[\mu_{A_\alpha}\cdot(t-d)] \qquad if \;\; g_- > 0 \end{aligned} \tag{110}$$

$$\begin{aligned} I_4 + I_5 + I_6 &= E_1[g_+\cdot(t-d)] + E_i(|g_-|\cdot d) + ln\left(\frac{g_+}{|g_-|}\right) + \\ &+ e^{\frac{\mu_{B_\beta}\cdot d}{\cos(\psi_{det})}} E_1(\mu_{A_\alpha}\cdot d) - e^{-\frac{\mu_{B_\beta}\cdot(t-d)}{\cos(\psi_{det})}} E_1[\mu_{A_\alpha}\cdot(t-d)] \qquad if \;\; g_- < 0 \end{aligned} \tag{111}$$

$$\begin{aligned} I_4 + I_5 + I_6 &= E_1[2\mu_{A_\alpha}\cdot(t-d)] + ln(2\mu_{A_\alpha}d) + \gamma + \\ &+ e^{\frac{\mu_{B_\beta}\cdot d}{\cos(\psi_{det})}} E_1(\mu_{A_\alpha}\cdot d) - e^{-\frac{\mu_{B_\beta}\cdot(t-d)}{\cos(\psi_{det})}} E_1[\mu_{A_\alpha}\cdot(t-d)] \qquad if \;\; g_- = 0 \end{aligned} \tag{112}$$

View Article Online
DOI: 10.1039/D4JA00463A

In this case, when $(t-d) \to 0$ the results for the three possibilities are:

$$I_4+I_5+I_6 = ln\left(\frac{\mu_{A\alpha}}{g_-}\right) - E1(g_- d) + e^{\frac{\mu_{B_\beta} \cdot d}{\cos(\psi_{det})}} E_1(\mu_{A_\alpha} \cdot d) \qquad if \;\; g_- > 0 \tag{113}$$

$$I_4+I_5+I_6 = ln\left(\frac{\mu_{A\alpha}}{|g_-|}\right) + Ei(|g_-|d) + e^{\frac{\mu_{B_\beta} \cdot d}{\cos(\psi_{det})}} E_1(\mu_{A_\alpha} \cdot d) \qquad if \;\; g_- < 0 \tag{114}$$

$$I_4+I_5+I_6 = ln(\mu_{A_\alpha} d) + \gamma + e^{\frac{\mu_{B_\beta} \cdot d}{\cos(\psi_{det})}} E_1(\mu_{A_\alpha} \cdot d) \qquad if \;\; g_- = 0 \tag{115}$$

As in the previous case, it is also important to address the potential extreme conditions having $\mu_{A_\alpha} \to 0$ while $(t-d)$ is not too small. As before the two situations that may be addressed are $|g_-| \to 0$ and $g_- < 0$. In the first case, the result of the sum of integrals is 0 as was also for the condition $d <= t/2$. In the case of $g_- < 0$ the result is:

$$\lim_{\mu_{A_\alpha} \to 0} (I_4+I_5+I_6) = E_1[b \cdot (t-d)] + E_i(b \cdot d) + e^{b \cdot d} ln(\frac{\mathscr{C}_{off}}{d}) - e^{-b \cdot (t-d)} ln(\frac{\mathscr{C}_{off}}{t-d}) \tag{116}$$

If now also $(t-d) \to 0$ applies, the limit of this eq(**??**) must be used, the result being:

$$\lim_{\substack{\mu_{A_\alpha} \to 0 \\ (t-d) \to 0}} (I_4+I_5+I_6) = \left(e^{b \cdot d} - 1\right) \cdot ln(\frac{\mathscr{C}_{off}}{d}) \tag{117}$$

4.4 The general layered target case

If the target is more complex than a single homogeneous layer and made up of several physically distinct layers as drawn schematicaly in fig.(**??**), calculating secondary fluorescence processes for PIXE experiments becomes a bit more complex and, as far as the author knows, this work is the first time a systematic, general global solution is presented in standard literature.

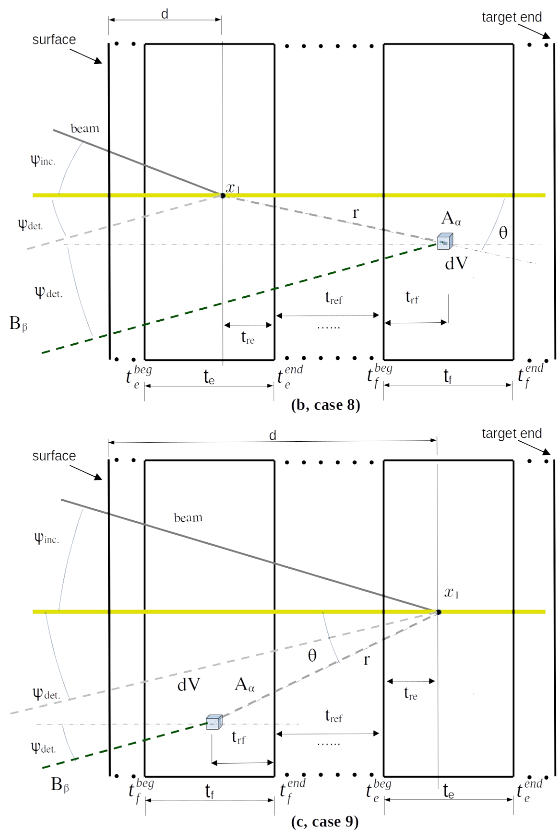

Figure 2 Primary X-rays A_α produced at a penetration depth x_1 in layer t_e originate the emission of secondary X-rays B_β in volume dV in layer t_f. These will look as if produced at depth x_1, and will either enhance B_β X-rays target yield from layer t_e or create a "*phantom*" presence of element B in layer t_e. (b) Case 8, the secondary fluorescence is produced in a physical layer present deeper into the target than the layer emitting the primary X-rays. (c) Case 9, the secondary fluorescence is produced in a physical layer present less deep in the target than the layer emitting the primary X-rays. In both cases it is once again assumed that the sample layers are homogeneous and infinite in the plane perpendicularly to the sample normal (shown in yellow).

In this case, three different situations can be faced in respect to secondary fluorescence: (a) the primary X-rays layer is the same as the layer emitting secondary X-rays, (b) the layer emitting secondary X-rays is deeper into the target than the primary X-rays layer or (c) the layer emitting secondary X-rays is closer to the target surface than the primary X-rays layer.

In case (a, or 7 since it follows integral I_6) eqs(**??**) and (**??**) nead just a slight change to cope with the extra layers that may be present between the emitting layer and the target surface, the result being:

$$\text{Case } a \text{ (or 7) : making } \mathscr{Q}^{7,n_f}_{B_\beta, A\alpha}(x_1) = \mathscr{Q}_{B_\beta, A\alpha}\left(x_1 - \frac{t_f^{beg}}{cos(\psi_{inc})}\right) \text{ based on eq(??)}$$

$$\chi^{7,n_f}_{B_\beta}(x_1) = \left(\prod_{i=1}^{n_f-1} e^{-\frac{\mu^i_{B_\beta} t_i}{cos(\psi_{det})}}\right) \sum_{\substack{allA\alpha \\ \text{inducing } B_\beta}} \sigma^X_{A\alpha, Z_i}(E(x_1)) f_A \, \mathscr{Q}^{7,n_f}_{A\alpha, B_\beta}(x_1) \tag{118}$$

In cases (b, or 8) and (c, or 9) the situation is different because it is necessary to account for three facts, namely: (i) the primary A_α X-rays absorption between the emission point x_1 and the absorption volume V_{fl} is not homogeneous, (ii) the B_β X-rays path from the integration volume up to the surface of the layer where secondary fluorescence effects are taking place has a different expression than the one defined in eq(**??**) used for the case of the single homogeneous layer and case (a) of multilayered targets, and (iii) a single more complex integral expression applies.

Table 2 Integration limits for r and θ for the integrals I_8 and I_9. The integral limits are the same due to the fact that the angle θ was defined as the smallest angle to the normal, in both cases.
* the value of $\mathscr{L}$ is an *ad hoc* cut-off taken as the value above which less than 5% of primary X-rays exit the emision layer.

	s	t^s_{re}	t^s_{ref}	t^s_{rf}
$d < t_f^{beg}$	8 (b)	$t_e^{end} - d$	$t_f^{beg} - t_e^{end}$	$r \cdot cos(\theta) - (t^8_{re} + t^8_{ref})$
$d > t_f^{end}$	9 (c)	$d - t_e^{beg}$	$t_e^{beg} - t_f^{end}$	$r \cdot cos(\theta) - (t^9_{re} + t^9_{ref})$
	$r_{s,min}$	$r_{s,max}$	$\zeta_i = \cos\theta_i$	$\zeta_f = \cos\theta_f$
$d < t_f^{beg}$	$\frac{t^8_{re}+t^8_{ref}}{\cos(\theta)}$	$\frac{t^8_{re}+t^8_{ref}+t_f}{cos(\theta)}$	1	$\mathscr{L}$*
$d > t_f^{end}$	$\frac{t^9_{re}+t^9_{ref}}{\cos(\theta)}$	$\frac{t^9_{re}+t^9_{ref}+t_f}{cos(\theta)}$	1	$\mathscr{L}$ *

In cases (b) and (c) eqs(**??**) and (**??**) need to be re-written. In order to simplify the expressions both for easy reading, but also for a clear understanding of its meaning, some definitions are presented in Table **??**.

Based on these and in fig.**??**, eq(**??**) can be promptly adjusted (note that t^s_{re} is the fraction of emiting layer crossed by A_α X-rays, and t^s_{rf} is the fraction of layer absorbing the A_α X-ray, crossed by these) leading to the following results:

$$d\mathscr{Q}^{8,n_f}_{B_\beta A\alpha}(x_1, r, \theta) = \frac{\mu^\eta_{\rho B_\beta}(A_\alpha)}{4\pi} \cdot e^{-\mu_{ne,A\alpha} \cdot \frac{t^8_{re}}{cos(\theta)}} \cdot \left(\prod_{i=n_e+1}^{n_f-1} e^{-\mu_{i,A\alpha} \cdot \frac{t_i}{cos(\theta)}}\right) \cdot$$
$$\cdot e^{-\mu_{nf,A\alpha} \cdot \frac{t^8_{rf}}{\cos(\theta)}} \cdot T^{n_f}_{8,B_\beta}(r,\theta) \sin(\theta) \; dr \, d\theta \, d\phi \tag{119}$$

$$d\mathscr{Q}^{9,n_f}_{B_\beta A\alpha}(x_1, r, \theta) = \frac{\mu^\eta_{\rho B_\beta}(A_\alpha)}{4\pi} \cdot e^{-\mu_{ne,A\alpha} \cdot \frac{t^9_{re}}{cos(\theta)}} \cdot \left(\prod_{i=n_e-1}^{n_f+1} e^{-\mu_{i,A\alpha} \cdot \frac{t_i}{cos(\theta)}}\right) \cdot$$
$$\cdot e^{-\mu_{nf,A\alpha} \cdot \frac{t^9_{rf}}{cos(\theta)}} \cdot T^{n_f}_{9,B_\beta}(r,\theta) \sin(\theta) \; dr \, d\theta \, d\phi \tag{120}$$

$$T^{n_f}_{8,B_\beta}(r,\theta) = \left(\prod_{i=1}^{n_f-1} e^{-\mu_{i,B_\beta} \cdot \frac{t_i}{cos(\psi_{det})}}\right) e^{-\mu_{n_f,B_\beta} \cdot \frac{t^8_{rf}}{\cos(\psi_{det})}} \tag{121}$$

$$T^{n_f}_{9,B_\beta}(r,\theta) = \left(\prod_{i=1}^{n_f-1} e^{-\mu_{i,B_\beta} \cdot \frac{t_i}{cos(\psi_{det})}}\right) e^{-\mu_{n_f,B_\beta} \cdot \frac{t_f - t^9_{rf}}{\cos(\psi_{det})}} \tag{122}$$

The following expressions replaces eq(**??**):

$$\chi^{s,n_f}_{B_\beta}(x_1) = \sum_{\substack{allA\alpha \\ \text{inducing } B_\beta}} \sigma^X_{A\alpha, Z_i}(E(x_1)) f_A \, \mathscr{Q}^{s,n_f}_{B_\beta A\alpha}(x_1) \tag{123}$$

being in this case, $$\mathscr{Q}^{s,n_f}_{B_\beta A\alpha}(x_1) = \iiint_{V_{n_f}} d\mathscr{Q}^{s,n_f}_{B_\beta A\alpha}(x_1, r_f, \theta) \tag{124}$$

View Article Online
DOI: 10.1039/D4JA00463A

Integrating the above differential expressions having the integral limits defined in Table(**??**) provides:

$$\mathscr{Q}^{8,n_f}_{B_\beta A_\alpha}(x_1) = \frac{\mu^{\eta}_{\rho B_\beta}(A_\alpha)}{2} \cdot e^{-\frac{\Sigma_{i=1}^{n_f-1}\left(\mu_{i,B_\beta}\cdot t_i\right)-\mu_{n_f,B_\beta}\cdot(t^8_{re}+t^8_{ref})}{cos(\psi_{det})}} \cdot \int_{\theta_i}^{\theta_f}\int_{r_{s,min}}^{r_{s,max}} e^{-\mu_{n_f,B_\beta}\left[\frac{r\cos(\theta)}{\cos(\psi_{det})}\right]} \cdot e^{-\frac{\mu_{ne,A\alpha}t^8_{re}+\Sigma_{i=ne+1}^{n_f-1}\left(\mu_{i,A\alpha}t_i\right)}{cos(\theta)}} \cdot e^{-\mu_{n_f,A\alpha}\left[r-\frac{t^8_{re}+t^8_{ref}}{\cos(\theta)}\right]} \sin(\theta)\, d\theta\, dr \tag{125}$$

$$\mathscr{Q}^{9,n_f}_{B_\beta A_\alpha}(x_1) = \frac{\mu^{\eta}_{\rho B_\beta}(A_\alpha)}{2} \cdot e^{-\frac{\Sigma_{i=1}^{n_f-1}\left(\mu_{i,B_\beta}\cdot t_i\right)+\mu_{n_f,B_\beta}\cdot\left[t_f+(t^9_{re}+t^9_{ref})\right]}{cos(\psi_{det})}} \cdot \int_{\theta_i}^{\theta_f}\int_{r_{s,min}}^{r_{s,max}} e^{\mu_{n_f,B_\beta}\left[\frac{r\cos(\theta)}{\cos(\psi_{det})}\right]} \cdot e^{-\frac{\mu_{ne,A\alpha}t^9_{re}+\Sigma_{i=n_f+1}^{ne-1}\left(\mu_{i,A\alpha}t_i\right)}{cos(\theta)}} \cdot e^{-\mu_{n_f,A\alpha}\left[r-\frac{t^9_{re}+t^9_{ref}}{\cos(\theta)}\right]} \sin(\theta)\, d\theta\, dr \tag{126}$$

or,

$$\mathscr{Q}^{8,n_f}_{B_\beta A_\alpha}(x_1) = \frac{\mu^{\eta}_{\rho B_\beta}(A_\alpha)}{2} \cdot e^{-\frac{\Sigma_{i=1}^{n_f-1}\left(\mu_{i,B_\beta}\cdot t_i\right)-\mu_{n_f,B_\beta}\cdot\left(t_f^{beg}-d\right)}{cos(\psi_{det})}} \cdot \int_{\theta_i}^{\theta_f}\int_{r_{s,min}}^{r_{s,max}} e^{-\left[\mu_{n_f,A\alpha}+\frac{\mu_{n_f,B_\beta}\cos(\theta)}{\cos(\psi_{det})}\right]r} \cdot e^{-\frac{\mu_{ne,A\alpha}t^8_{re}+\Sigma_{i=ne+1}^{n_f-1}\left(\mu_{i,A\alpha}t_i\right)-\mu_{n_f,A\alpha}\left(t_f^{beg}-d\right)}{cos(\theta)}} \sin(\theta)\, d\theta\, dr \tag{127}$$

$$\mathscr{Q}^{9,n_f}_{B_\beta A_\alpha}(x_1) = \frac{\mu^{\eta}_{\rho B_\beta}(A_\alpha)}{2} \cdot e^{-\frac{\Sigma_{i=1}^{n_f-1}\left(\mu_{i,B_\beta}\cdot t_i\right)+\mu_{n_f,B_\beta}\cdot\left[t_f+\left(d-t_f^{end}\right)\right]}{cos(\psi_{det})}} \cdot \int_{\theta_i}^{\theta_f}\int_{r_{s,min}}^{r_{s,max}} e^{-\left[\mu_{n_f,A\alpha}-\frac{\mu_{n_f,B_\beta}\cos(\theta)}{\cos(\psi_{det})}\right]r} \cdot e^{-\frac{\mu_{ne,A\alpha}t^9_{re}+\Sigma_{i=n_f+1}^{ne-1}\left(\mu_{i,A\alpha}t_i\right)-\mu_{n_f,A\alpha}\left(d-t_f^{end}\right)}{cos(\theta)}} \sin(\theta)\, d\theta\, dr \tag{128}$$

Further simplification will result from applying the following change of variables to the integration eqs(**??**) and (**??**):

$$\zeta = cos(\theta)\ ;\ d\zeta = -\sin(\theta)d\theta\ ; \tag{129}$$

$$\aleph^8(\zeta) = \mu_{n_f,A\alpha} + \frac{\mu_{n_f,B_\beta}}{\cos(\psi_{det})}\zeta\ ;\ \aleph^9(\zeta) = \mu_{n_f,A\alpha} - \frac{\mu_{n_f,B_\beta}}{\cos(\psi_{det})}\zeta \tag{130}$$

Which using the changes of variable mentioned results in:

$$\mathscr{B}^8_{ne,n_f} = \sum_{i=1}^{n_f-1}\left(\mu_{i,B_\beta}\cdot t_i\right) - \mu_{n_f,B_\beta}\cdot\left(t_f^{beg}-d\right)$$

$$\mathscr{B}^9_{ne,n_f} = \sum_{i=1}^{n_f-1}\left(\mu_{i,B_\beta}\cdot t_i\right) + \mu_{n_f,B_\beta}\cdot\left[t_f+\left(d-t_f^{end}\right)\right]$$

$$\mathscr{C}^8_{ne,n_f} = \mu_{ne,A\alpha}\cdot t^8_{re} + \sum_{i=ne+1}^{n_f-1}\left(\mu_{i,A\alpha}\cdot t_i\right) - \mu_{n_f,A\alpha}\left(t_f^{beg}-d\right)$$

$$\mathscr{C}^9_{ne,n_f} = \mu_{ne,A\alpha}\cdot t^9_{re} + \sum_{i=n_f+1}^{ne-1}\left(\mu_{i,A\alpha}\cdot t_i\right) - \mu_{n_f,A\alpha}\left(d-t_f^{end}\right)$$

$$\mathscr{Q}^{s,n_f}_{B_\beta A_\alpha}(x_1) = \frac{\mu^{\eta}_{\rho B_\beta}(A_\alpha)}{2} \cdot e^{-\frac{\mathscr{B}^s_{ne,n_f}}{cos(\psi_{det})}} \cdot \int_{\zeta_i}^{\zeta_f}\int_{r_{s,min}}^{r_{s,max}} -e^{-\aleph^s(\zeta)\cdot r} \cdot e^{-\frac{\mathscr{C}^s_{ne,n_f}}{\zeta}} dr\, d\zeta \quad ; \quad d = x_1\cdot cos(\psi_{det})$$

therefore:

$$\mathscr{Q}^{s,n_f}_{B_\beta A_\alpha}(x_1) = \frac{\mu^{\eta}_{\rho B_\beta}(A_\alpha)}{2} \cdot e^{-\frac{\mathscr{B}^s_{ne,n_f}}{cos(\psi_{det})}} \cdot \int_{\zeta_i}^{\zeta_f}\left(\frac{e^{-\aleph^s(\zeta)\cdot r}}{\aleph^s(\zeta)}\right)\Bigg|_{r_{s,min}}^{r_{s,max}} \cdot e^{-\frac{\mathscr{C}^s_{ne,n_f}}{\zeta}}\, d\zeta \tag{131}$$

which leads to the following integrals that are solved numerically using gaussian methods.

$$\mathscr{Q}^{s,n_f}_{B_\beta A_\alpha}(x_1) = \frac{\mu^{\eta}_{\rho B_\beta}(A_\alpha)}{2}\int_{\zeta^s_i}^{\zeta^s_f} -\left[\frac{e^{-\frac{\aleph^s(\zeta)}{\zeta}\left(t^s_{re}+t^s_{ref}\right)}}{\aleph^s(\zeta)} - \frac{e^{-\frac{\aleph^s(\zeta)}{\zeta}\left(t^s_{re}+t^s_{ref}+t_f\right)}}{\aleph^s(\zeta)}\right] \cdot e^{-\left(\frac{\mathscr{C}^s_{ne,n_f}}{\zeta}+\frac{\mathscr{B}^s_{ne,n_f}}{cos(\psi_{det})}\right)} d\zeta = $$

$$= \frac{\mu^{\eta}_{\rho B_\beta}(A_\alpha)}{2}\int_{\mathscr{L}^*}^{1}\frac{1-e^{-\frac{\aleph^s(\zeta)\cdot t_f}{\zeta}}}{\aleph^s(\zeta)} \cdot e^{-\left(\frac{\aleph^s(\zeta)\left(t^s_{re}+t^s_{ref}\right)+\mathscr{C}^s_{ne,n_f}}{\zeta}+\frac{\mathscr{B}^s_{ne,n_f}}{cos(\psi_{det})}\right)} d\zeta \tag{132}$$

All terms in the exponential having been grouped together to avoid numerical integration problems.

The final expression for the number of B_β X-rays emitted by a layered target, which structure may be simulated by a set of layers parallel to the surface, and infinite in the directions perpendicular to the sample normal, becomes:

$$N^{ml}_{B_\beta}(E_p) = \frac{\Omega}{4\pi}\ \varepsilon_{\det,B_\beta}\ T_{sis,B_\beta}\ N_p\ C_{pp}(E_p)\, b_{cs}\ \mathscr{Y}^{tot,ml}_{B_\beta} \tag{133}$$

being

$$\mathscr{Y}^{tot,ml}_{B_\beta}(E_p) = \frac{\mathscr{C}_{part}}{M_{at,B}}\ \sigma^X_{B_\beta}(E_p)\,\xi^{scf,ml}_{eq,B_\beta}(E_p) \tag{134}$$

$$\xi^{scf,ml}_{eq,B_\beta}(E_p) = \sum_{m=1}^{All\ layers}\left(\prod_{k=1}^{m-1}T^k_{B_\beta}\right)\frac{\sigma^X_{B_\beta}\left(E^m_p(x^m_0)\right)}{\sigma^X_{B_\beta}(E_p)} \cdot f_{B,m} \cdot \int_{x^m_0}^{x^m_{(E_{out})}}\frac{\sigma^X_{B_\beta}\left(E_p(x)\right)T^m_{B_\beta,Z_i}(x)}{\sigma^X_{B_\beta,Z_i}\left(E^m_p(x^m_0)\right)}\, dx + \int_{x^m_0}^{x^m_{(E_{out})}}\frac{\chi^{s,m}_{B_\beta,ml}(x)}{\sigma^X_{B_\beta,Z_i}\left(E^m_p(x^m_0)\right)}\, dx \tag{135}$$

where, with $\mathscr{Q}^{s,ne}_{B_\beta A_\alpha}(x_1)$ provided by eq(**??**), $\chi^{s,ne}_{B_\beta,ml}(x)$ is:

$$\chi^{s,ne}_{B_\beta,ml}(x) = \sum_{n_f=1}^{\substack{all\ B_\beta\\ emitting\ layers}}\left[f_{B,n_f}\cdot\sum_{A\alpha,ne=1}^{\substack{all\ A\alpha,ne\\ inducing\ B_\beta}}\sigma^X_{A\alpha}\left(E^{ne}_p(x)\right)f_{A,ne}\ \mathscr{Q}^{s,ne}_{B_\beta A_\alpha}(x)\right] \tag{136}$$

It is important to realise that solving eqs.(**??**) numerically, adds an extra set of sums to the ones already originated from eq(**??**), combined with eq(**??**), which must be carefully implemented.

Notice that now, because the mass fraction term must be included in the definition of the equivalent thickness, it cannot be just put in evidence as was done in eq(**??**).

This is not a problem for simulations, but is a complex situation to address if the problem in question is the exact fitting of spectra of unknown samples. In the present work, this issue is not addressed beyond this statement, still it is a subject that will be addressed in the frame of the applications part of the present trilogy.

5 The general case expression

Summing up all previous results, it is possible to write a global expression for the most general case possible, namely for the PIXE yield of a wide spot or wide detector that requires a generalized sum over a set of (y_a, z_b) pairs.

It is nevertheless important to assure that homogeneous conditions are respected within each partial spot (y_a, z_b), as otherwise the expression cannot be used without detailed adaptations that have not been presented in this paper, even if they may eventually be derived from the results presented here.

Starting from eqs(**??**) to (**??**) and adding up the secondary fluorescence terms the final result is:

$$N_{j,Z_i}(E_p) = \sum_{(y_a,z_b)=1}^{All\ (y_a,z_b)\ pairs}\frac{\Omega^{(y_a,z_b)}}{4\pi}\ \varepsilon^{(y_a,z_b)}_{\det,j}\ T^{(y_a,z_b)}_{sis,j}\ N^{(y_a,z_b)}_p\ C_{pp}(E_p)\, b_{cs}\ \mathscr{Y}^{ml,(y_a,z_b)}_{j,Z_i} \tag{137}$$

being

$$\mathscr{Y}^{ml,(y_a,z_b)}_{j,Z_i}(E_p) = \frac{\mathscr{C}_{part}}{M_{at,Z_i}}\ \sigma^X_{j,Z_i}(E_p)\,\xi^{ml,(y_a,z_b)}_{eq,j,Z_i}(E_p) \tag{138}$$

and

$$\xi^{ml,(y_a,z_b)}_{eq,j,Z_i}(E_p) = \sum_{m_{(y_a,z_b)}=1}^{All\ layers}\Bigg\{\left(\prod_{n_{(y_a,z_b)}=1}^{m_{(y_a,z_b)}-1}T^{n_{(y_a,z_b)}}_{j,Z_i}\right)\frac{\sigma^X_{j,Z_i}\left(E_p^{m_{(y_a,z_b)}}\right)}{\sigma^X_{j,Z_i}(E_p)}\,f^{m_{(y_a,z_b)}}_{Z_i} \cdot \left[\int_{x_0^{m_{(y_a,z_b)}}}^{x^{m_{(y_a,z_b)}}_{(E_{out})}}\frac{\sigma^X_{j,Z_i}(E(x))\cdot T^{m_{(y_a,z_b)}}_{j,Z_i}(x)+\chi^{h,m_{(y_a,z_b)}}_{j,Z_i;(B_\beta)}(x)}{\sigma^X_{j,Z_i}\left(E_p^{m_{(y_a,z_b)}}\right)}\, dx\right] + \sum_{n_{f(y_A,z_b)}=1}^{\substack{All\ layers\\ \neq m_{(y_a,z_b)}}}\ \sum_{\substack{allA\alpha\\ inducingB_\beta}}\chi^{n_f,m_{(y_a,z_b)}}_{j,Z_i;(B_\beta)}(x)\Bigg\} \tag{139}$$

In this equations, $\chi^{h,m_{(y_a,z_b)}}_{j,Z_i;(B_\beta)}(x)$ refers to the homogeneous cases and case a (or 7) of eq.(**??**) and $\chi^{n_f,m_{(y_a,z_b)}}_{j,Z_i;(B_\beta)}(x)$ refers inter layers secondary fluorescence, cases b and c (or 8 and 9) described by eq(**??**).

6 Implementation and analysis

6.1 Homogeneous targets

Once obtained these results, its computational implementation is reasonably straightforward, the single item needing some attention being the cases where variables present very small values so that limit expressions must be used.

View Article Online
DOI: 10.1039/D4JA00463A

The implementation was made as additional code to the previous DT2 code[? ?], which was designed from the start to allow the handling of multilayered targets[?].

6.1.1 The infinite target case

In the infinite target case, eqs.(**??**) and (**??**) are used as long as the following expression is true:

$$d > 10^{-5} \;\wedge\; g_{-} > 10^{-5} \;\wedge\; \mu_{A\alpha} > 10^{-5} \tag{140}$$

If this expression is not true, than each condition must be taken into account individually. Table **??** lists the conditions, equations and limit cases replacement when dealing with infinite (thick) targets.

Table 3 Equations selection table for the case of infinite targets.

d	$\lvert g_{-}\rvert$	$\lvert g_{-}\rvert \cdot d$	$\mu_{A\alpha} \cdot d$	g_{-}	equation
$> 10^{-5}$	$> 10^{-5}$	–	$> 10^{-5}$	$g_{-} > 0$	eq(**??**)
				$g_{-} < 0$	eq(**??**)
			$\leq 10^{-5}$	$g_{-} < 0$	eq(**??**)
	$\leq 10^{-5}$	$> 10^{-5}$	$> 10^{-5}$	–	eq(**??**) $\equiv$ (**??**)
			$\leq 10^{-5}$	–	$ln(2)$
		$\leq 10^{-5}$	$> 10^{-5}$		eq(**??**)
			$\leq 10^{-5}$	–	$ln(2)$
$\leq 10^{-5}$	$> 10^{-5}$	$> 10^{-5}$	$> 10^{-5}$	–	$ln\left(\frac{g_{+}}{\mu_{A\alpha}}\right)$
			$\leq 10^{-5}$	$g_{-} < 0$	eq(**??**)
		$\leq 10^{-5}$	_	_	$ln(2)$
	$\leq 10^{-5}$	–	–	–	$ln(2)$

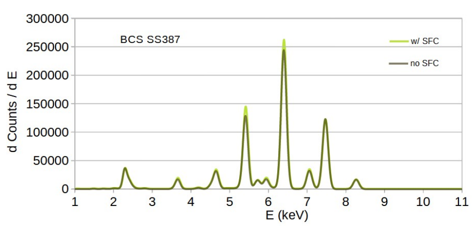

Figure 3 Overlap of spectra simulation of 1.65 MeV proton irradiation of BCS_SS387 reference material taking into account secondary fluorescence corrections (w/ SFC) and not considering these (No SFC). It can be seen that differences are observable in the most intense peaks, but not so much in the others. In this case, the most intense SFC effect is observed in Cr at 5.4 keV, which presents an effect of 11.6% , while Fe at 6.4 keV presents a SFC effect of 7.4%.

The simulations corresponding to one of the alloy cases presented in the 1992 paper[?] is shown in fig.(**??**). In this case the BCS S387 iron nickel standard was considered. Spectra shown correspond to simulations assuming a proton beam irradiation using an energy of 1.65 MeV, which were the conditions used in the experimental data collected for the 1992 paper. Simulations were also carried out for proton beams of 1.1 MeV and 2.5 MeV. In fig.(**??**) the changes in percentage correction determined as function of beam energy are presented for the five elements regarding which effects are more significant. It can be seen that as ion beam energy increases, also the necessary correction increases. Results are different from those presented in the 1992[?] paper because the present work uses a penetration function method and gaussian integration, which accounts for the whole sample, as used in the 1996 paper[?] and not a Simpson integration over pairs of irradiated numerical layers (similar to Ahlberg et al. method[?]) used in 1992. The present results for this homogeneous thick target are, therefore, identical to those found in the 1996 paper. Applying the corrections factors presented in fig.(**??**) for 1.65MeV, to the experimental data published in table 3 of ref.[?], relative differences of 1.7%, 0.78%, 5.0% and 1.33% are found now between secondary fluorescence corrected data and reference values for Ti, Cr, Mn and Fe respectively. Taking into account that the reference values have uncertainties of 4%, 0.64%, 5.0% and 0.55% respectively, it can be concluded that the results obtained after secondary fluorescence correction fully agree with the standard reference data.

Secondary fluorescence correction situations may, nevertheless, be significantly different from this. Testing as examples some potentially complex cases such as MoP, PbCrO4, Ti82.5-Mo10-Mn2.5 and Co10-Cu90, for 1.65 MeV proton irradiations, different cases can be observed.

In the case of low energy X-rays, namely P-K, Mo-L and Pb-M, no meaningful secondary fluorescence corrections are observed, the most intense case being Mo-L_{β_1} that showns an 1.86% increase for an irradiation of a bulk Ti82.5-Mo10-Mn2.5. The difference in energy between Pb L lines and Cr-K absorption edge results also in the fact that photo-electric absorption cross section is too low for a significant effect to be observable in PbCrO4.

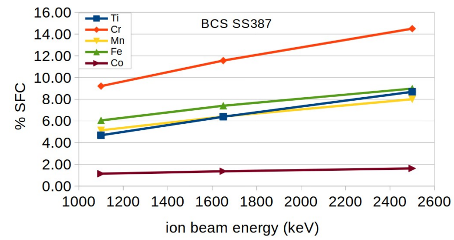

Figure 4 Change of the percentage of secondary fluorescence correction (% SFC) counts on the total counts in the area of the X-ray peaks simulated for five different chemical elements, as function of the proton beam energy. It can be seen that for all these cases, the %SFC increases as ion beam energy increases.

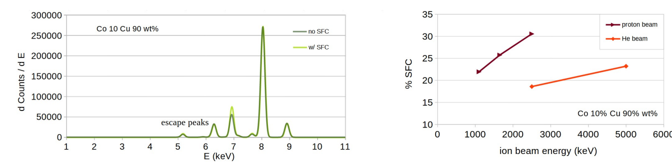

Figure 5 Simulation of 10wt% cobalt alloy in copper overlap of SFC corrected and not corrected spectra (left) and change of the percentage of secondary fluorescence correction (% SFC) counts on the total counts in the area of the Co X-ray peaks simulated as function of the proton and He beam energy. It can be seen that the %SFC increases as function of ion beam energy is stronger for proton beams than for the He beams.

In the Co10-Cu90 case, a different situation applies and secondary fluorescence corrections for Co K_α lines from 18% to 30% are found. The effect visible in the Co K_α peak height, for a proton irradiation at 1.65MeV, is shown in fig.(**??**).

6.1.2 The half-thick target case

In the case of the half-thick targets, as shown in section 3.3, calculations are a bit more complex, and therefore so is the implementation. The equations selection for this case is resumed in Tables **??** and **??**, since two different sets of sums of integrals must be dealt with.

Table 4 Equations selection table for the sum $I_1 + I_2 + I_3$ (primary emission point located before the layer half-thickness) for the case of homogeneous half-thick layer targets.

$d <= t/2$	$\lvert g_{-}\rvert$	$\lvert g_{-}\rvert \cdot d$	$\mu_{A\alpha} \cdot d$	g_{-}	equation
$> 10^{-5}$	$> 10^{-5}$	–	$> 10^{-5}$	$g_{-} > 0$	eq(**??**)
				$g_{-} < 0$	eq(**??**)
			$\leq 10^{-5}$	$g_{-} < 0$	eq(**??**)
	$\leq 10^{-5}$	–	$> 10^{-5}$	–	eq(**??**)
			$\leq 10^{-5}$	–	0
$\leq 10^{-5}$	$> 10^{-5}$	$> 10^{-5}$	$> 10^{-5}$	–	eq(**??**)
			$\leq 10^{-5}$	$g_{-} < 0$	eq(**??**)
		$\leq 10^{-5}$	_	_	0
	$\leq 10^{-5}$	–	–	–	0

Applying these to the simulation of the most intense case shown in the previous section, namely the cobalt copper alloy, it can be seen that the secondary fluorescence correction in thin targets is not zero, but it decreases significantly with thickness as well as with ion beam energy.

In fig.(**??**) it can be seen that the secondary fluorescence correction increases as function of the beam energy (as was already seen for thick targets) as well as the target thickness.

Although not shown in the graph, He 2500keV are fully stopped in 3.2 and 6.4 mg/cm^2 targets, and the same happens to He 5000keV and proton 1100keV beems in the 6.4 mg/cm^2 target. Still, out of these four cases, only for the He 2500keV in the 6.4 mg/cm^2 target is the secondary fluorescence correction identical to that of the thick target.

This results from the fact that secondary fluorescence effects that take place beyond the ion beam range, still affect the overall spectra.

View Article Online
DOI: 10.1039/D4JA00463A

Table 5 Equations selection table for the sum $I_4 + I_5 + I_6$ (primary emission point located beyond the layer half-thickness) for the case of homogeneous half-thick layer targets.

$t-d <= t/2$	$\lvert g_-\rvert$	$\lvert g_-\rvert(t-d)$	$\mu_{A_\alpha}(t-d)$	g_-	equation
$> 10^{-5}$	$> 10^{-5}$	–	$> 10^{-5}$	$g_- > 0$	eq(??)
				$g_- < 0$	eq(??)
			$\leq 10^{-5}$	$g_- < 0$	eq(??)
	$\leq 10^{-5}$	–	$> 10^{-5}$	–	eq(??)
			$\leq 10^{-5}$	–	0
$\leq 10^{-5}$	$> 10^{-5}$	–	$> 10^{-5}$	$g_- > 0$	eq(??)
				$g_- < 0$	eq(??)
			$\leq 10^{-5}$	$g_- < 0$	eq(??)
	$\leq 10^{-5}$	–	–	–	eq(??)

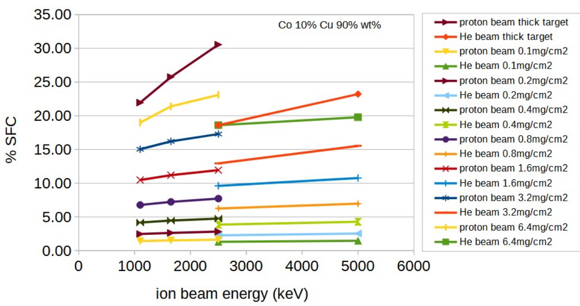

Figure 6 Simulation of 10wt% cobalt alloy in copper change of the percentage of secondary fluorescence correction (% SFC) counts of the total counts in the area of the Co X-ray peaks as function of the beam energy and target tickness.

6.2 Layered targets

If the target is not thick enough but composed of more than a single homogeneous layer, secondary fluorescence may be induced in the same region or in regions different from the one where the primary X-rays are emitted.

As presented in the previous section, the complexity of the case makes that in the second case, the integrals involved must be solved numerically.

The first of these cases, which involves calculating secondary fluorescence effects taking place in the same physical layer as the primary X-rays emission, is handled using eq(**??**) and appart the absorption term and the shift of the penetration value by the layer surface reference, nothing is changed relative to the homogeneous half-thick layer target case.

The second of these two conditions involves the emission of secondary fluorescence X-rays from layers different from that emitting the primary X-rays.

In this case, two conditions can be faced, namely that the layer emitting secondary X-rays is deeper than that emitting the primary X-rays, or the other way around.

In each of these situations, eq(**??**) applies and the single numerical extreme issue that must be overcome is the vanishing value of the cossines, which is dealt with by setting an *ad-hoc* cut-off as mentioned in Table **??**.

The extreme values problem being a minor one in this case, it is still necessary to take into account and overcome a large list of embedded sums that needs to be managed for the proper implementation of the geral case calculation.

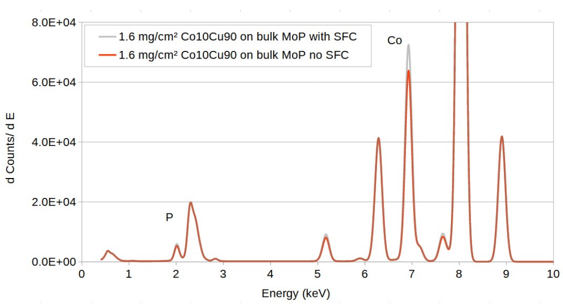

Figure 7 Simulation of a 1.6 mg/cm^2 film of 10wt% cobalt alloy in copper placed on top of a bulk MoP substrate.

In order to illustrate these type of conditions, simulations were run for a combination of layers and subtrate materials of MoP and Co10-Cu90 alloy. As shown, in the case of MoP bulk, secondary fluorescence induced on P by Mo-L lines is small relative to the direct primary induction of X-rays in P. If a film of Co10-Cu90 alloy is set on top of it, no much difference is observed even though the secondary fluorescence in P raises to roughly 11 %. In fig.**??** the effect of a 1.6 mg/cm^2 film of Co10-Cu90 placed on top of a bulk MoP substrate is shown.

Still, if the order of the materials is exchanged, a different image can be found. In fig.**??** the change of effect observable as function of the top layer thickness is presented for both the MoP layer on top as well as the other way around, aside of the comparison of the simulation of spectra of a sequence of MoP and Co10-Cu90 0.8 mg/cm^2 films multilayer starting by MoP, and three times less charge.

It can be seen that important differences are observed. A systematic validation of these results is necessary to assure that both theoretical work and software implementation are working properly, before systematic use of the results here present are possible. Still, the report of this validation will be presented in part II.

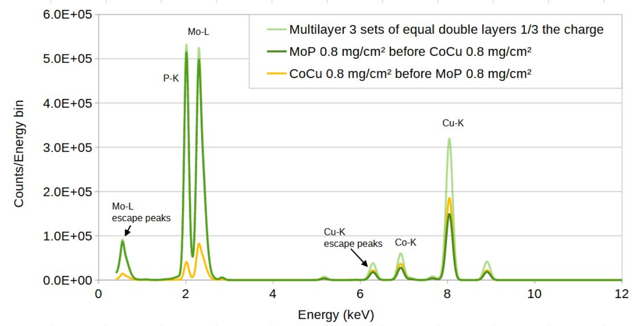

Figure 8 Spectra of 0.8mg/cm^2 MoP film on top of an 0.8mg/cm^2 Co10-Cu90 film a Co10-Cu90 film on top of a MoP film and a multilayer sequence of 3 pairs of MoP/Co10-Cu90 films. The differences can be seen to be very significative, as expected.

7 Conclusions

Simulation of PIXE spectra is a useful tool for various purposes, from the simplest one of lecturing PIXE without access to an accelerator to its unavoidable use for analysis of data from Total-IBA[?] experiments.

PIXE spectra reproduction is available from a few computer codes described in the literature, such as GUPIX[?], GeoPIXE[?] or LibCPIXE[?] but as far as the author is aware of, up until the present paper, no computer code available was able to deal with simulation and secondary fluorescence corrections of multilayer samples where the same chemical element may be present in more than one layer.

As far as the author is also aware, a general and global theory here presented to deal with X-ray induced secondary X-ray fluorescence in PIXE experiments in so general conditions was also not available in standard and easy accessible literature before this work.

The present algorithms are implemented in the new version of the DT2 code (DT2F_0v9_98), corresponding therefore to a major upgrade of its prior versions[??].

Conflict of interests

The author has no conflict of interests related to this work.

Data availability

Data used in the present work is in total data generated by the revised version of the DT2 computer code mentioned in the conclusions section. At the present moment, the generated data used in this work is available just upon request to the author. Still, in a near future, eventually still before the final publication of this work, a repository will be created for it and the possibility to make available the simulation software as freeware code is under evaluation. In face of a positive response to this evaluation, the freeware version of the executable and using conditions will be made available at the same repository.

Acknowledgements

The global PIXE secondary X-ray fluorescence corrections theory and its computational implementation which I assume might have been missing an equivalent in PIXE standard and easy accessible literature for a long time now, was requested several times by Chris Jeynes as a needed key-stone for the PIXE component in Total-IBA[?]. A special acknowledgement is therefore due to him since his pressure for it was one of the important drives for carrying out such a long, detailed and necessary work. Even though in many pratical situations faced the effect in complex multilayered targets is small, as shown, situations do emerge where that is not so, and in any case, uncertainty budgets calculations do need the results present in this work even for the conditions where the correction is small.

The present work was partially funded by the FCT UID/Multi/04349/2020 project.

View Article Online
DOI: 10.1039/D4JA00463A

Dr. Miguel A. Reis
Centro de Ciências e Tecnologias Nucleares
Instituto Superior Técnico, Universidade de Lisboa
Campus Tecnológico e Nuclear,
Estrada Nacional 10, km 139,7
2695-066 BOBADELA LRS
PORTUGAL

e-mail: mareis@ctn.tecnico.ulisboa.pt
tel.:+351-219946107

Bobadela, 17th December 2024

Data availability statement for the manuscript entitled:
Multilayer targets PIXE spectra simulation (X,X) secondary fluorescence corrections algorithm

Data used in the present work is in total data generated by the revised version of the DT2 computer code mentioned in the conclusions section. At the present moment, the generated data used in this work is available just upon request to the author. Still, in a near future, eventually still before the final publication of this work, a repository will be created for it and the possibility to make available the simulation software as freeware code is under evaluation. In face of a positive response to this evaluation, the freeware version of the executable and using conditions will be made available at the same repository.